LiDAR point-cloud mapping of building façades for building energy performance simulation

O'Donnell, J.; Truong-Hong, Linh; Boyle, N.; Corry, Edward; Cao, Jun; Laefer, Debra F.

DOI
10.1016/j.autcon.2019.102905

Publication date
2019

Document Version
Accepted author manuscript

Published in
Automation in Construction

Citation (APA)
O'Donnell, J., Truong-Hong, L., Boyle, N., Corry, E., Cao, J., & Laefer, D. F. (2019). LiDAR point-cloud mapping of building façades for building energy performance simulation. *Automation in Construction*, *107*, Article 102905. https://doi.org/10.1016/j.autcon.2019.102905

LiDAR point-cloud mapping of building façades for building energy performance simulation

James O'Donnell[a], Linh Truong-Hong[b], Niamh Boyle[a], Edward Corry[a,e], Jun Cao[d], Debra F. Laefer[c,f]

[a] *School of Mechanical and Materials Engineering and UCD Energy Institute, University College Dublin, Belfield, Dublin 4, Ireland*
[b] *Department of Geoscience and Remote Sensing, Delft University of Technology, 2628 CN, Delft, The Netherlands*
[c] *Urban Modelling Group, School of Civil Engineering, University College Dublin, Belfield, Dublin 4, Ireland*
[d] *E3D,RWTH Aachen, Aachen, Germany*
[e] *Mary Immaculate College, Limerick, Ireland*
[f] *New York University, New York, USA*

Abstract

Current processes that create Building Energy Performance Simulation (BEPS) models are time consuming and costly, primarily due to the extensive manual inputs required for model population. In particular, generation of geometric inputs for existing building models requires significant manual intervention due to the absence, or outdated nature of available data or digital measurements. Additionally, solutions based on Building Information Modelling (BIM) also require high quality and precise geometrically-based models, which are not typically available for existing buildings. As such, this work introduces a semi-automated BEPS input solution for existing building exteriors that can be integrated with other related technologies (such as BIM or CityGML) and deployed across an entire building stock. Within the overarching approach, a novel sub-process automatically transforms a point cloud obtained from a terrestrial laser scanner into a representation of a building's exterior façade geometry as input data for a BEPS engine.

Email addresses: `james.odonnell@ucd.ie` (James O'Donnell), `l.truong@tudelft.nl` (Linh Truong-Hong), `niamh.boyle.1@ucdconnect.ie` (Niamh Boyle), `edward.corry@mic.ul.ie` (Edward Corry), `cao@e3d.rwth-aachen.de` (Jun Cao), `debra.laefer@nyu.edu` (Debra F. Laefer)

Preprint submitted to Automation in Construction *August 8, 2019*

Semantic enrichment is performed manually. This novel solution extends two existing approaches: (1) an angle criterion in boundary detection and (2) a voxelisation representation to improve performance. The use of laser scanning data reduces temporal costs and improves input accuracy for BEPS model generation of existing buildings. The approach is tested herein on two example cases. Vertical and horizontal accuracies of 1% and 7% were generated, respectively, when compared against independently produced, measured drawings. The approach showed variation in accuracy of model generation, particularly for upper floors of the test case buildings. However, the energy impacts resulting from these variations represented less than 1% of the energy consumption for both cases.

Keywords: Light Detection And Ranging (LiDAR), Laser Scanning, City-Scale Modelling, Building Energy Performance Simulation (BEPS), Retrofit, Semi-Automated Façades Generation

---

1. Introduction

The advantages of creating and using Building Energy Performance Simulation (BEPS) models for existing buildings are well known. Such models can be used during design to predict energy usage, calibrated to reflect current building consumption, and employed to aid optimisation procedures [1]. However, there is a significant performance gap between predicted and actual performance for the majority of existing buildings [2, 3, 4] - implying limitations of existing models - which may be ascribable to discrepancies in their geometric representation. Other BEPS related factors include modelling assumptions, modeller errors, calculation errors within the programme and the absence of model updates that mirror changes to the building over its life cycle. Typically, BEPS models are associated with the design phase of the building life-cycle (BLC) and are not usually updated to reflect changes that occur to the building over time [5]. In cases where the model has been updated to reflect such changes in the physical building and its operations and subsequently calibrated, BEPS models have been shown to be instrumental in achieving greater operational efficiency [6]. Furthermore, as a decision making tool, BEPS models can compare alternatives during retrofit design scenarios [7]. Consequently, such tools are desperately needed as countries struggle to meet carbon emission and energy consumption targets within the context of the existing building stock.

For example, within Europe, authorities predict that 80% of the current building stock will still exist in 2050. Thus, scalable solutions must be developed to serve the extensive retrofitting market associated with these buildings [8]. BEPS tools can serve as an enabling mechanism for the improved operational performance of such buildings and groups of buildings [9]. Unfortunately, the process of creating relevant models is complex, expensive, and time consuming and involves the manual input of a significant amount of data [10]. Automating the process of entering building geometry into BEPS tools could be a critical motivator to encourage building practitioners to use such tools throughout the BLCs of existing buildings.

Notably, there have been many recent advances in automated building model generation, particularly in BIM based solutions, whereby BIM geometry is traced over a point cloud captured by laser scanning, also known as Light Detection and Ranging (LiDAR). In BIM based solutions, the model is generated in BIM authoring tools such as Revit or ArchiCAD or through hybrid methods. Such hybrid methods tend to have significant manual input requirements [11, 12] and are, thus, not easily extendable to district-level or city-level investigations. Additionally, while the hybrid approaches have been used in an energy optimisation context, solutions using point clouds have not been used as a basis for automated geometric parameter input within the BEPS sphere, despite its widespread availability for building groups [13] and its potential impact in facilitating cost-effective BEPS models of individual buildings.

From a BEPS model development perspective, the key issue is the creation of the BEPS geometry [14]. Automated and semi-automated solutions aim to ease the burden for BEPS modellers, but such approaches require precisely defined inputs in a BIM format such as IFC [15, 16, 17]. Thus, creating a BIM for an existing building, especially with the view to BEPS modelling is a challenging task. Given the nature and need for large-scale building retrofits and a parallel move towards interlinked digital models that capture and represent the built environment over time, proposed solutions must concentrate on efficient and cost-effective BEPS model development. Such a model must represent a building's status and be updated with relative ease to account for retrofit design alternatives, thereby, allowing for the quantification of the proposed impact of individual and combined retrofit measures, as well as changes in user behaviours. To date, leveraging LiDAR data for BEPS has not been considered feasible for energy simulation tools. Although Garwood et al. [18, 19] presented interesting advances and a large-scale case study in the area of point cloud processing, their process requires manual intervention during the interpretation of the point cloud data. Since the fundamental inputs for BEPS tools are two-dimensional (2D) planes representing zone surfaces enclosed by a series of connected lines, BEPS tools are incapable of interpreting a point cloud associated with its attributes without post-processing. Traditional approaches use intermediary programmes, especially those that are based on Computer Aided Drawing (CAD) programs. However, they require significant manual intervention to convert point clouds into the lines and planes required for BEPS inputs, and production difficulties may arise due to having to manage massive quantities of data points.

Several methods have been developed to automate the reconstruction of internal building components, e.g. walls, doors, ceilings and floors. For example, Budroni et al. proposed a plane-based sweep algorithm to detect the walls, ceilings and floors [20]. In this implementation, the vertical sweep initially extracted horizontal planes, and vertical walls were detected using a horizontal sweep. By using the advantages of a voxelisation model, Valero et al. decomposed a point cloud into a voxel space [21]. By examining the distribution of voxels in the horizontal plane, the floors and ceilings were contained a large number of voxels, and the point clouds within these voxels became inputs for the floors and ceilings. The remaining data points were projected onto a 2D horizontal plane to create a binary image. The walls were then identified by using a Hough Transform. An approach presented by Sanchez et. al. extracted point clouds of floors, ceilings and walls by using normal vectors of the points [22]. Then alpha shapes were used to fit the floors, ceilings and walls. In contrast, Shi et. al. combined a region-based segmentation and model-based segmentation to extract building surfaces [23].

In summary, the cost for reconstructing a 3D building model is still high. For example, when Garwood et. al. combined external and internal scanning to reconstruct building geometry and to determine the thickness of the building components (e.g. thickness of the walls and ceilings or floors), the process took several weeks to create a 3D geometry model using Leica Cyclone software [19]. In response, this paper proposes a seamless, efficient, and robust process for generating geometrically accurate models for BEPS from terrestrial laser scanning data. Notably, the proposed method can work with multiple building shapes and components and can overcome missing data.

This paper addresses current research gaps that persist when using intermediate data formats such as IFC or gbXML, as further transformation processes from these formats have limitations that result in data loss and errors when applied at scale. IFC to BEPS tools are currently at the prototype stage only and require consistent, high quality inputs. They are, therefore, not sufficiently robust. As a result, such approaches are not yet ready for wide-scale deployment. Approaches that first map to gbXML prior to energy modelling have a systematic limitation, as gbXML uses the centre-line for representation of geometry. In the context of energy simulation in buildings, this centre-line convention typically results in discrepancies in calculated surface areas and volumes, which significantly exceed standard engineering tolerances and cause over estimations of building energy consumption, as defined by Bazjanac et. al. [24].

Consequently, the aim of this work is to develop a new methodology for extracting the exterior geometry of a building appropriate for BEPS modelling. This is to be achieved through the use of a terrestrial laser scanner (TLS) and an automatic, seamless, scalable, and robust method for reconstructing 3D building models without any third party software or manual intervention. This representation is subsequently transformed using a short, semi-automatic process into a format that is directly usable for building energy performance simulation. In doing so, the proposed solution overcomes many limitations such as (1) incorrect geometric representations in gbXML and (2) extremely precise geometric definitions in the IFC format when processing IFC for energy modelling conversions. In this case, the transformation is for BEPS modelling of existing buildings. The semi-automated nature of the approach represents an important step towards deploying BEPS modelling across groups of buildings, an important consideration as cities move towards interlinked digital representations of all building assets. The remainder of the paper is organised into five sections.

Section 2 describes the state-of-the-art in this area, while Section 3 outlines the methodology behind the semi-automated process for building façade generation. The novel method to transform the resulting data into the format required for building simulation purposes is then illustrated (Section 4). The validation methods for the models are discussed, and a demonstration of the process is given (Section 5). Finally, in Section 6, conclusions, limitations, and possible future work in this area are addressed.

2. Related Work

Western societies have a pressing need for scalable, building-specific solutions that address a largely energy inefficient building stock [8]. Recent developments in the area of building innovation for energy use reduction have primarily focused on identifying retrofitting measures, while dismissing the use of BEPS tools because of the cost, time, and effort needed to develop and calibrate such models. Additionally, BEPS tools typically generate entity-averaged outputs, as opposed to identifying localised discrepancies [25] (i.e. average wall heat flux (W/m^2), or identifying wall segments with poor insulation levels). However, BEPS can be an enormously useful tool when evaluating a range of retrofit alternatives. Since the goal of the paper is to develop an automatic process to create 3D building models for BEPS from LiDAR data, the related work section is restricted to the creation of 3D building thermal profiles and building energy modelling. Input data for those purposes can be thermographic imagery and/or laser scanning data. For other aspects relating to building energy modelling, readers are referred elsewhere (e.g. Cho et al. [10]).

Three-dimensional building thermal profiles

Increasingly, efforts to visualise building energy at a city scale are being undertaken. Two notable projects of significant size include the Energy Atlas Berlin [26] and SEMANCO [27]. Both projects predict a rudimentary annual energy usage for each building within the study area. The Berlin project includes approximately 500,000 buildings [26]. The geometric building models were created from a combination of aerial laser scanning (ALS) data and 2D footprints, that were then textured with photographs of the building façade. In contrast, the SEMANCO project proposed a platform supporting improved energy analysis based on existing data, which was applied to three urban areas with a combined population exceeding 150,000 people [27]. In this project, a set of tools were also developed to automatically create 3D maps from aerial photography and a digital earth model (DEM) or digital terrain model (DTM), with the corresponding energy usage integrated for visualisation. In related work, López et al. [28] presented a complete methodology for generating thermographic 3D point clouds of urban areas by using a thermographic camera to acquire thermal data and mobile laser scanning to collect building topography. Similarly, a combination of TLS data and aerial ortho-photography was used to manually create 3D building models with level of detail (LoD) 2 for computational fluid dynamics (CFD) analysis to estimate temperatures in urban environments [29], but the method proved time consuming in both data acquisition and building model generation.

In an effort to explore detailed energy consumption of the building, Lagüela et al. [30] mapped thermal images onto the point cloud of the building to measure energy efficiency directly. Similarly, González-Aguilera et al. [31] textured thermographic images onto a 3D point cloud of a building, which was generated from matching thermographic images. Lagüela et. al.. [32] textured as-built models with RGB and thermographic images to diagnose and analyse building energy usage. The proposed method created the building model as a set of intersection lines between the building surfaces, where the doors and windows were not included. Focusing on interiors, Borrmann et al. [33] used a mobile robot to integrate a thermal camera and laser scanning sensor for automatic data acquisition and generated a full thermal model of a building's interior. Additionally, Cho and Wang [34] used a TLS and a thermal camera to generate 3D point cloud models for building envelopes with the corresponding temperature values at the individual point level.

Significant research initiatives have developed efficient methods to create accurate 3D building energy profiles, but these methods do not explicitly exploit building geometry. As such, the models for mapping thermal information therein cannot be used directly in energy tools. Work in that area is described in the next section.

Building Energy Modelling

A geometric building model is a crucial part of BEPS. With recent developments in point cloud acquisition and processing, 3D geometric building models have the potential to support building energy modelling. However, in practice, 2D geometric information is still primarily used for energy modelling. For example, Moran et al. [35] applied the Passive House Planning Package tool to assess energy usage and CO_2 emissions in historic buildings in the city of Bath. For that effort, manually collected, 2D geometric data of building components were used. Similarly, to evaluate energy retrofitting results, Morelli et al. [36] created building envelopes of existing structures by employing the software Be10, where the geometric building model was derived from building planning documents.

Three-dimensional building models are increasingly being used to improve the accuracy of energy simulation. For example, Ham and Goparvar-Fard [37] evaluated predicted building energy performance derived from a combination of CFD and EnergyPlus software against actual measurements from digital and thermal imagery. Thermal image information was mapped onto building models created from a large number of digital images, which allowed users to visualise and compare actual measurements and simulated results in a common 3D environment. Several automatic algorithms have been developed to create either exterior or interior 3D building models, but certain limitations persist: (1) primarily applicable to relatively simple buildings [38]; (2) require a priori knowledge [39]; and/or (3) give relatively low geometric accuracy [40]. Amongst the methods for exterior building model reconstruction, Zolanvari and Laefer [41] recently proposed a slicing method to divide the building façade into the number of independence horizontal and vertical strips. The points of the strip were then compressed into line segments, and the end points of the line segments were known as boundary points. The method provides relatively high levels of accuracy for the boundary points and single façades but does not create automatically complete building models. Similarly, Li et al. detected the corners of openings based on the gradient of the number of points within the sliding window search along both horizontal and vertical directions [42]. Although the method can work properly for a case of partial missing data, it is limited for façades with rectilinear and repetitive openings.

Moreover, with a recent demand for BIM and indoor navigation, recent methods mostly focus on generating indoor building models but accurate detection and generation of openings (doors and windows) is still difficult for older and complex structures [43]. For example, in reconstructing openings from interior point clouds, Adan and Huber used the Hough transform to detect boundary lines based on boundary points of openings extracted from an binary image of a wall [44]. This work reported an average absolute error of 5.39cm for window dimensions with a standard deviation of 5.70cm when compared to the ground truth. Díaz-Vilariño et al. generated building models from TLS data that had door and window errors typically ranging from 2.8% to 6.5%, with a maximum error of 34.3% [40]. Wang and Cho used data points on the edges of the building and its windows for BEPS tools [45] . However, the generated building geometry had a relatively low accuracy with average errors of around 16.9% and 12.5% for the window widths and lengths, respectively.

Jung et al. used boundary tracing to extract boundary points of interior walls and openings from binary images [46]. Subsequently, a constrained least-squares adjustment approach generated boundary lines from these boundary points – the accuracy of the interior building components depends on grid size and threshold distances. The study also calculated a root mean square error (RMSE) between a 3D wireframe model's vertices and a ground truth derived from total station measurement of about 4.8cm. Tamke et al. used supervised learning techniques to detect and classify openings from a point cloud of interior building walls [47]. The method can detect openings with a success rate 91.2% for doors and 72.8% for the windows but with 39.5% classification error. The extracted doors and windows averaged 9.8% smaller than ground truth in a terms of area. Ochmann et al. presented a method that can detect openings with an accuracy about 85.2% [48]. As an alternative, Quintana et al. decomposed a point cloud into voxels, which are classified as occupied, occluded and opening voxels [49] and used Otsu's global histogram threshold technique and the Canny edge detector to identify openings from colour and depth images, respectively. An accuracy of 98.3% in terms of opening areas was achieved, but only for rectangular openings. Similarly, Jung et al. converted the point cloud of wall segments into a binary image to detect hollow areas potentially representing openings and boundaries [43]. The shape and size of the hollow areas were used to remove incorrect openings. The algorithm successfully generated all walls and detected all openings but was sensitive to grid cell size. The study reported root mean square errors between reference points and reconstructed wall vertices of 8.9cm and 7.4cm but detailed geometric accuracy of openings was not been reported.

By deploying a spatial representation, Staats [50] used a voxelisation model to detect doors for indoor navigation from handheld indoor laser scanning data. The doors were detected with a high fluctuation of voxels in both vertical and horizontal directions. The authors determined that the method can detect about 84.2% actual doors. Li et al. decomposed a point cloud of a story into cells and the line fitting was used to create the wall edges from a binary image of the wall [51].The maximum errors varied from $4.29 \pm 0.53 cm$ to $45.74 \pm 5.52 cm$ in terms of distance between vertices, or from -0.86 m^2 to 4.51 m^2 in terms of area.In the worst case, the algorithm detected about 82% of the walls and doors in the model.

In other related work, Tran et al. proposed a shape grammar to generate 3D indoor building models through a simple primitive and interactive grammar rules [52]. Although the method can reconstruct building elements for various data sets through a visual evaluation, the method still requires manual adjustment for the locations of histogram peaks and correction of the classification labels. Shi et al. combined region-based segmentation for wall with openings and predefined opening dimensions were used to eliminate false positives [23]. Although that method can detect the number of openings, geometric accuracy was not been reported. Moreover, in an attempt to explore the backpack scanning data for indoor modelling, Wang et al. used an α-shape based method to extract the boundary points of each façade, and a k-mean clustering method was used to extract potential lines of doors and windows from internal lines of the wall [53]. Like many others, this algorithm is applicable only for rectangular openings. Finally, to overcome limited availability of laser scanning data for buildings, Neuhausen and König [54] detected windows from images through two main steps. First, a machine learning method extracted the windows but the detection accuracy was quite low, at about 69%. To improve the detection rate in the second step, the authors applied an image-based edge detection technique to extract the windows' boundary lines. Next, a knowledge base using window patterns in the façade and detected windows in a previous step were used to detect missing windows. This implementation improve the detected rate to 95.2%. However, the accuracy of the window size may be limited, because the authors defined the boundary lines of the window from the average of a set of edges detected from regions surrounding the window.

In current practice, building energy usage estimation usually differs from the actual energy performance [45]. This can occur for reasons that include comparisons using as-designed building models (as opposed to as-built building models) or building models with a low level of detail (LoD), thus resulting in significant geometric discrepancies between the input model and the actual operational building. For example, when an LoD2 building model is used, openings (i.e. doors and windows) are not explicitly modelled. When a LoD3 model with the major external features such as doors, windows, and a correct roof shape is used, it must be transformed for use in BEPS software; see [55] for a more detailed set of definitions for various LoDs. However, achieving this at scale has not been realisable to date.

Although significant complementary information can be added to geometric models of buildings, the initial creation of a building geometry is most commonly done through a manual process that is both time consuming and expensive. Recent advances in laser scanning and photogrammetry based techniques for building reconstruction offer more opportunities for developing as-built building models for the purposes of BEPS. Nonetheless, a robust, efficient, automatic workflow for accurate 3D building model reconstruction has remained a significant challenge; this is particularly true in the case of a detailed BEPS model requiring the geometry of the building including a cross section and coordinate information for floors, walls, ceilings, roofs, columns, and doors.

3. Method

The goal of the proposed method is to automatically process point cloud data for building façades into a format usable by all BEPS tools with minimal manual intervention; the method was validated by testing on one BEPS engine (EnergyPlus). The process also includes validation of simulation input and a mechanism to check geometric configurations through visualisation of DXF files, which are generated by the target BEPS tool. The proposed method has two key sub-processes (Figure 1): (1) point cloud data capture and processing to create 3D geometric building models from terrestrial laser scanning data (Section 3.1) and (2) BEPS creation (Section 4.1).

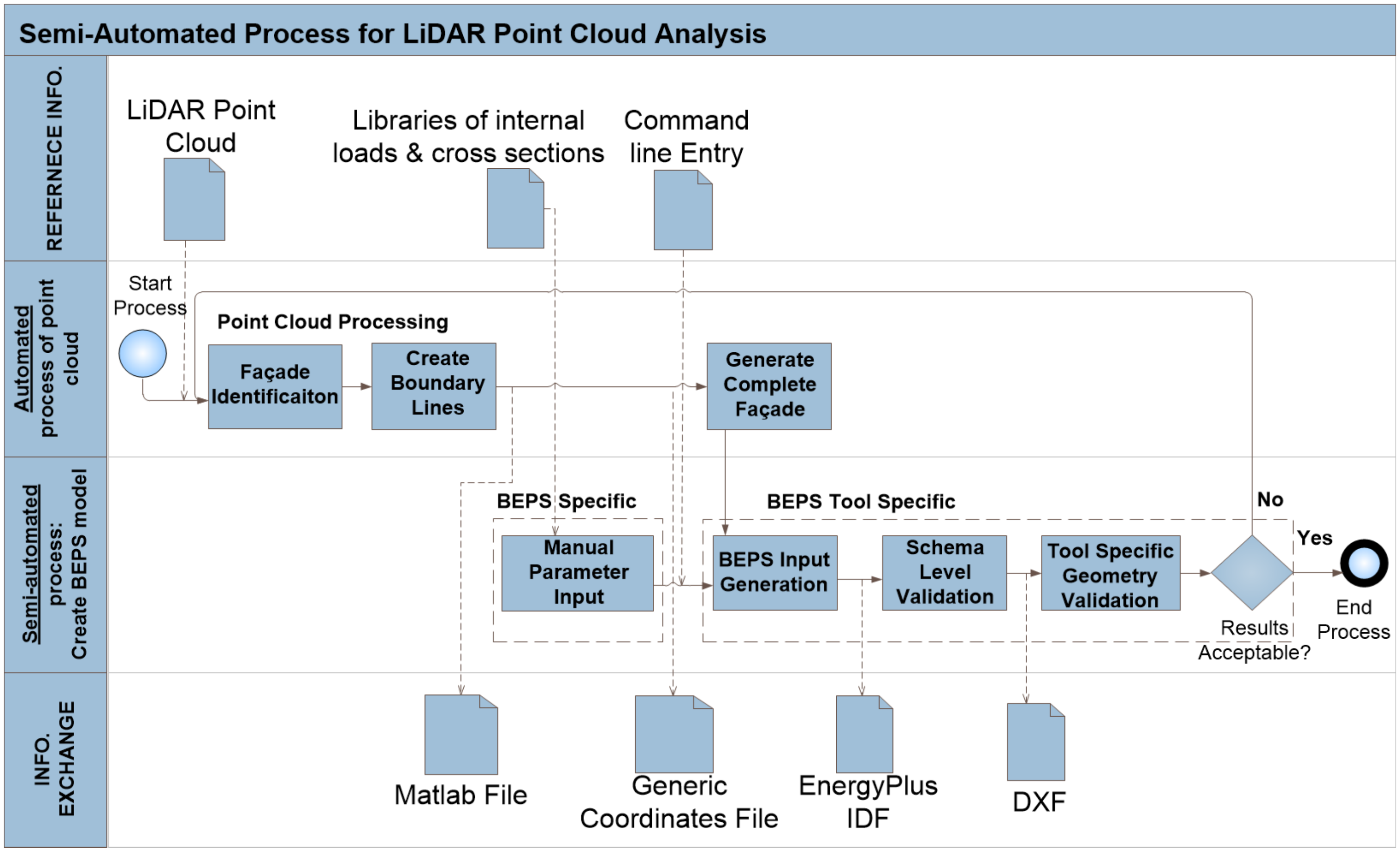

Figure 1: Process Diagram representing a semi-automated workflow that converts point cloud information into a format compatible with BEPS tools

3.1. Point cloud processing

Processing the point cloud consists of three main steps, as illustrated in Figure 2: (1) extraction of a portion of a point cloud capturing the façade of the building from the scanned data points; (2) creation of boundary lines of the façade and its openings (i.e. doors and windows), which are based on points on their boundaries, and (3) creation of a 3D geometric model of the building façades. This work presumes that building features reside within vertical walls and that doors and windows are primarily glass-plated or are recessed. For the purpose of this work, architectural details were intentionally ignored.

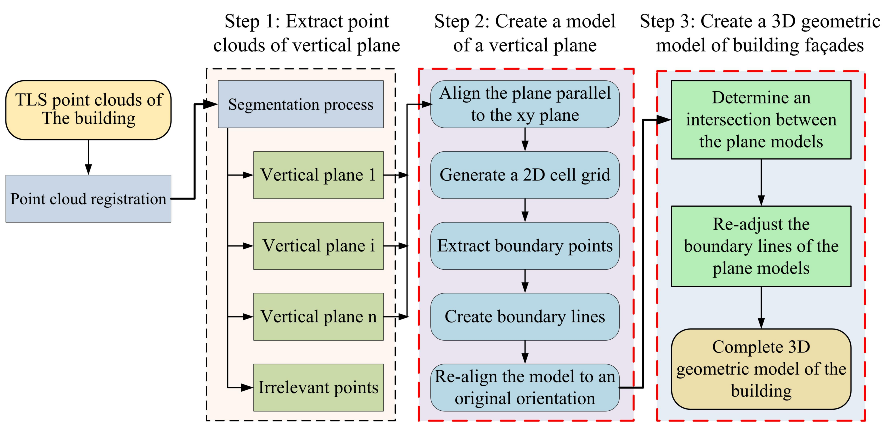

Figure 2: Proposed method for façade reconstruction using laser scanning data

The workflow begins with the registration of multiple point clouds of the building, acquired from different point of views due to footpath limitations and obstacles. The registration process can be done through using artificial targets or objects' features (e.g. edges or corners of façade planes). In practice, the registration was done by using the scanner's proprietary software, for example, Leica Cyclone for the Leica scanners or RealWorkSurvey for Trimble scanners [56], which took less than 5 minutes to register 3 to 5 point clouds. Next, the point cloud of the building with x-, y-, and z- coordinates was exported as input data for the proposed method.

The resulting registration included a large amount of redundant points including those of interior components, terrain, vehicles, and adjacent façades. Since the 3D building model generally involves multiple surfaces and complicated shapes, reconstructing building models from the full set of data points remains a large challenge. Step 1 uses a segmentation process to partition the 3D scene data points into multiple surfaces to create an input for Step 2. Although many segmentation methods can extract the point cloud of a building façade (e.g. [57, 58, 59]) significant user input or judgement is commonly needed to tune input parameters or filter spurious segments. In this work, a voxel-based region growing method [59] is employed to extract the data points on the same planar surface. This automatic approach relies heavily upon an octree indexing structure to separate the points into two groups: (1) building exterior and (2) other (e.g. internal building components, vehicles, or noise), which can be eliminated. For more details of the segmentation method, refer to Vo et al. [59]. Next, the point cloud of each façade or vertical plane is sequentially processed to identify boundary lines of a building and its features.

Since each vertical exterior surface of the building consists of a set of points, $\mathbf{P} = \{p_i, \text{i} = (1, . . ., \text{n})\} \in \text{R}^3$, boundary lines for its entirety and its features (doors and windows) are created from the data points **P** (Step 2). In this work, each exterior wall is assumed to be a vertical, largely flat surface, **S**. Next, the data points of the surface (**P**) are projected onto a plane parallel to the xy plane of the global coordinate system (GCS) by mapping principal directions of the fitting plane of the façade onto the unit vectors of the GCS, which are given in Equation 1. The principal directions or eigenvectors of each wall are determined by employing a principal component analysis (PCA) [60].

$$\left\{ \begin{array}{c} x \\ y \\ z \end{array} \right\} = R_z(\beta_3)R_y(\beta_2)R_x(\beta_1) \left\{ \begin{array}{c} X \\ Y \\ Z \end{array} \right\} \quad (1)$$

Herein, the data points of each wall are described as x-, y-, and z-coordinates in the GCS, where x and y axes are now, respectively, the horizontal and vertical directions of the wall, while the z coordinates of all points are the same (Figure 3a). The 3D model of each wall can be generated by extruding its 2D model in the x-y plane along the z-axis, with a predefined wall thickness.

In order to generate boundary lines of the façade and its openings (e.g. doors and windows), a 2D cell grid is employed to represent the decomposition of an entire façade into non-overlapping 2D regions, commonly referred to as cells (step 2.1). An initial bounding box of all projected points **P** can be defined by two pairs of coordinate values (x_{min}, y_{min}) and (x_{max}, y_{max}).

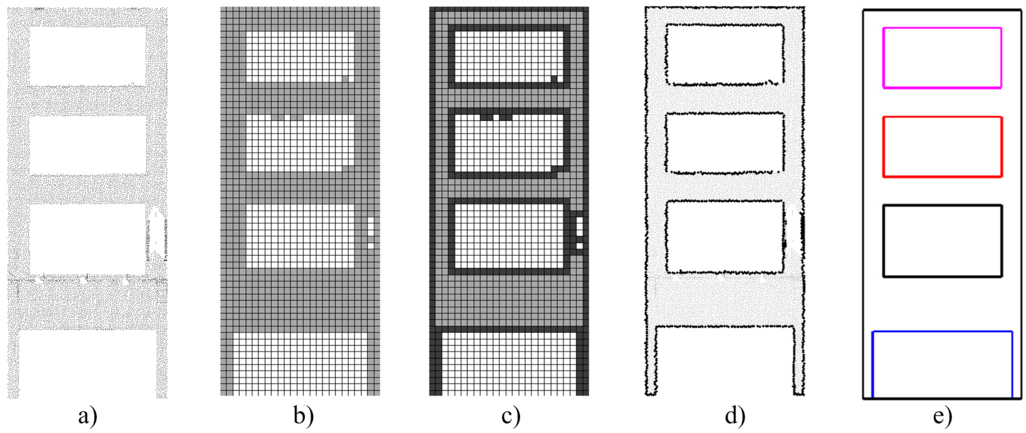

Figure 3: a) Input data b) Initial 2D cell grid c) Full cells containing candidate points d) Boundary points e) Boundary lines of the wall

Subsequently, a cell grid divides a bounded, 2D region into a set of regular cells by grids along the x- and y-axes in a Cartesian coordinate system. Each cell is described by an index, a geometry, and a property. The index is defined as c(i, j), where $i \in [1; N_x]$, $j \in [1; N_y]$, and N_x and N_y are defined in Equations (2) and (3). The geometry is stored as a centre $[x_{cen}, y_{cen}]$ and a cell size, while the property is either "full" or "empty" (described by 1 and 0, respectively). A cell is full, if it contains at least one data point. Otherwise, it is empty (Figure 3b).

In this method, the empty cells within the building wall are assumed to describe the inside of doors and windows or holes due to missing data. An opening is only detected, if one or more empty cells appear inside a candidate area for an opening. Thus, the predefined cell size plays an important role within the method proposed by this paper. If the cell size is too large, no empty cell may be available within the area of the door or window. On the other hand, if the cell size is too small, particularly if it is less than the sampling step of the data point, a number of empty cells may appear over the area of the building wall, which in turn lead to over-detection of openings. Truong-Hong and Laefer [61] proved that a predefined cell size of 0.2m is an appropriate value to generate at least one empty cell within doors and windows corresponding to a minimum opening size of 0.4m, as established from a survey of urban window sizes [62]. With a predefined cell size of 0.2m, the number of cells along the horizontal and vertical directions are given in

Equations 2 and 3.

$$N_x = \frac{x_{max} - x_{min}}{cell\_size} + 1 \tag{2}$$

$$N_y = \frac{y_{max} - y_{min}}{cell\_size} + 1 \tag{3}$$

Next, the process extracts points on boundaries of the façade and its openings. This is referred to as the boundary point extraction step. Although several other methods are potentially available (e.g half-disk criterion [63], triangulation mesh [64], multiple criteria [65]), in this work, an angle criterion [66] is employed to extract the boundary points from a set of candidate points. However, unlike previous work with an angle criterion (e.g. [66]), where all data points must be checked as to whether they are boundary points or not, the method herein only examines possible points (called candidate points), which are the data points in the vicinity of the boundaries of the wall and its openings. In the cell representation of the façade or wall (Figure 3b), the full cells containing the candidate boundary points of the doors/windows are connected to an empty cell group appearing as a hole inside the façade, while those of the façade boundary connect to the empty cell group along the outside of the façade and/or attach to the minimum bounding box of the data set. Extraction of the full cells possessing the candidate points is shown in (Figure 3c).

A candidate boundary point is a boundary point, if the maximum angle between two consecutive neighbour points exceeds an angle threshold by 90^o; for full details on the selection of the angle threshold and the process of extracting boundary points see Truong-Hong et al. [66]. Additionally, the selection of neighbour points differs from that proposed by Truong-Hong et al. [66], where a k-d tree was required for neighbour point searching. In this work, the process starts with a full cell (c(i, j)) containing a given point. Other full cells (c(k, l)) connected to c(i, j) are then extracted. The neighbour points of the given point are the rest of the data points within c(i, j) and all of the points within c(k, l).

Notably, due to occlusions, unrealistic holes may appear on the wall. In order to eliminate those holes, the height (H_0) and width (L_0) of each hole is computed from its boundary points and compared to dimensions of common openings in the building. A hole is considered a real opening, if its height and length satisfy the conditions expressed in Equation 4, where the minimum opening size is 0.4m [64, 38], and its height-to-width ratio varies from 0.25 to 5.0 [62]. Figure 3d highlights the process of distinguishing real from unrealistic openings and infilling the unrealistic openings.

$$f(H_0, L_0, \frac{H_0}{L_0}) = \begin{cases} H_0 \geqslant 0.4; L_0 \geqslant 0.4; 0.25 \leqslant H_0/L_0 \leqslant 5 : Opening \\ Otherwise : Non-opening \end{cases} \quad (4)$$

Next, a boundary line for a building component is created from the boundary points (Figure 4a). In the method proposed herein, boundaries of the building wall and associated openings are assumed to consist of a set of vertical, horizontal, and/or inclined lines. A region growing method is then adopted to separate the boundary points of the wall and its openings, in which the data points of each group are distributed on the same pattern (either vertical, horizontal, or inclined) (Figure 4b). As part of this, the tangent vector of each boundary point is computed from its k-nearest neighbour (kNN) points using PCA, for which a neighbourhood of 10 kNN points is recommended. The initial seeding point is selected from the boundary points; this point is chosen based on the smallest deviation angle between its tangent vector and a unit vector (n_y = [0,1,0]). If the angles between the seeding point and boundary points in the kNN point(s) are smaller than an angle threshold (recommended as 5° based on empirical trials), the kNN points are added iteratively into the seeding point group. This process is applied, until all boundary points are checked.

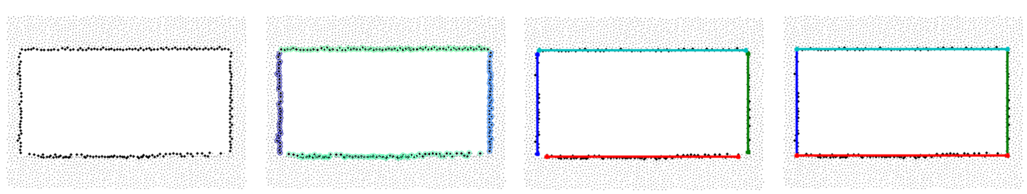

a) Boundary points of a window b) Boundary points of groups c) Boundary line generation d) Final boundary line

Figure 4: Illustration of boundary line generation for a building feature

Subsequently, each resulting group is classified as vertical, horizontal, and/or inclined for the purpose of creating the boundary lines of the building features. A tangent vector of the group is computed from the group's boundary points. The classification of the group's pattern is determined based on the deviation angle between the tangent vector of the group and the unit vector. If the deviation is less than the angle threshold, for example 5°, the unit vector is (n_y = [0,1,0]) for vertical and is (n_x = [1,0,0]) for horizontal. Otherwise, the group's pattern is classified as inclined. Notably, the group is only considered for further processing, if the length of its pattern is greater than or equal to half of the minimum opening size (0.4m) [61]. Then, boundary lines are generated from the boundary points of each group ($L = \{p_i = (x_i, y_i, z_i)|1 \leq i \leq k$) and the group's pattern classification. Vertical and horizontal patterns are expressed in Equations 5 and 6, respectively, while a least mean squares fitting [67] is applied to the inclined pattern (Figure 4c). Next, the boundary lines of each feature are adjusted to ensure continuity by extending or trimming the boundary lines at their intersection points (Figure 4d). The final boundary lines of the wall and its openings are shown back in Figure 3e. Geometric information for those boundary lines is in the plane parallel to the xy plane within the GCS, which is not the original orientation of the surface. Equation 1 is used to re-map the boundary lines into the original plane of the vertical surface or the façade.

For vertical patterns:

$$x_0 = \frac{\sum_{i=1}^{k} x_i}{k}; y_{min} = min(y_i); y_{max} = max(y_i) \tag{5}$$

For horizontal patterns:

$$y_0 = \frac{\sum_{i=1}^{k} y_i}{k}; x_{min} = min(x_i); x_{max} = max(x_i) \tag{6}$$

In reality, a building often contains multiple vertical surfaces or façades. After extracting the point cloud of each vertical wall (Step 1), the boundary lines of the wall and its openings are separately reconstructed using the procedure in Step 2. For example, with a point cloud of the building in Figure 5a, the segmentation process automatically extracted the point clouds of 2 vertical walls. The proposed method was applied to reconstruct boundary lines for each vertical wall shown in Figure 5c. However, there is a gap between two adjacent vertical walls because of (1) missing edge points during data acquisition [68], (2) the fact that segmentation methods do not allow edge points to belong to multiple segments (or walls), and (3) a procedure in which boundary line reconstruction takes the data points along boundaries of building components, which leads and shrinks them to the bounding box of the vertical wall (Figure 5c). Therefore, to reconstruct a 3D water-tight building model for BEPS, a new boundary line between two adjacent vertical surfaces must be created, instead of having two boundary lines (one for each vertical surface) (Figure 5b and c). The process starts by determining the parametric equation of the surface in the form of the centre and normal of the surface. From a set of vertices P_i (i = 1, . . . N, where N is the number of vertices) of the boundary lines, the surface centre is a centroid of P_i, while the surface normal is the eigenvector corresponding the smallest eigenvalue computed from a covariance matrix of P_i. Next, a pair of adjacent vertical walls (or façades), S_i and S_j, of the building can be determined based on the Euclidean distance $d(P_i, P'_i)$ horizontally, which is calculated from x and y coordinates of P_i and P'_i, where P_i and P'_i are respectively the boundary vertices of S_i and S_j (Figure 5c and d) [67]. In this implementation, if any $d(P_i, P'_i)$ is less than 1.4 times of the cell size, a pair of surfaces are judged to be adjoining vertical walls [69]. An intersection line is computed using the surface equations, in this example $S_1(q_1, n_1)$ and $S_2(q_2, n_2)$, where (q_1, n_1) and (q_2, n_2) are the centres and normal vectors. The result is shown in Figure 5d. Subsequently, the vertical boundary lines of S_1 and S_2 closest to the intersection line are replaced by the intersection line. Finally, the set of boundary lines of each surface is extended or trimmed to ensure a set of closed boundary lines for each vertical surface. Through this procedure the final reconstructed building model can be achieved as shown in Figure 5e. In addition, vertical gaps ranging from millimeters to centimeters may be present at the top of the adjacent facçades, which arise due to errors of data segmentation or boundary line reconstruction (Figure 5e). In order to overcome this issue, a possible solution is to retrieve boundary points used to generate boundary lines at the top of the facçades. A new surface (S_{atop}) can be generated through these boundary points, and the new boundary lines on the top of the facçade is an intersection line between the facçade surface and S_{atop}. This step will be fully implemented in future work.

At this stage, the 3D exterior building model comprises multiple polylines to represent boundaries of the building and its openings (doors and windows). The vertices for each surface are determined using two iterations: (1) the first stores vertices of the exterior polylines that represent the boundary of each surface and (2) the second iteration stores vertices of the interior polylines describing the boundary of the windows or doors belonging to the surface. If the surface has no opening, the second iteration fails to return any vertices. Both iterations have an ID that can be easily used to retrieve the geometric information of the surface for further processing.

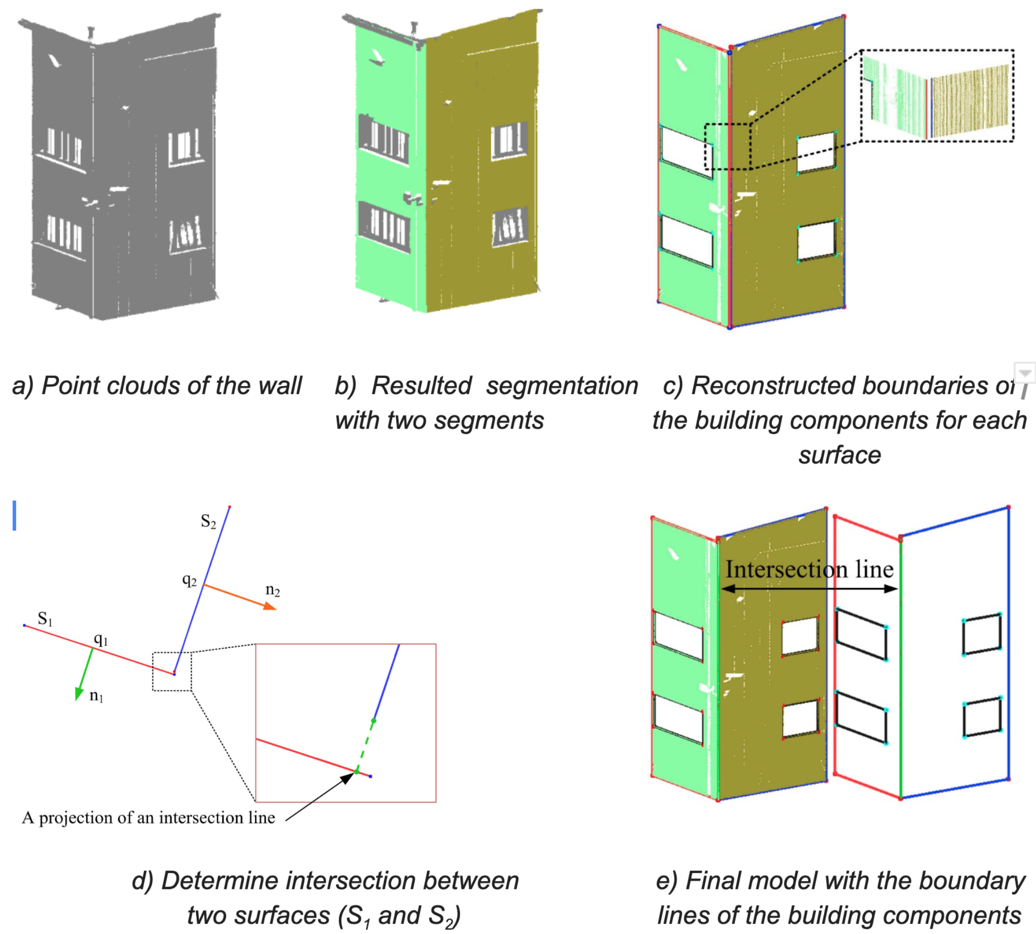

Figure 5: Process to overcome gaps between vertical surfaces of a building's exterior wall

Additional information including spatial and semantic information about the building and environment variables is required in order to simulate building energy use based on the exterior geometry of the building.

The next step (Section 4) transforms the processed point cloud and manually inserted data into the syntax required by the target BEPS engine, in this case, EnergyPlus.

4. BEPS Creation and Model Validation

This section describes the process of creating and validating a BEPS model. In line with the process illustrated in Figure 1, a number of sequential steps including defining a number of concise manual inputs that enable automatic conversion of the processed building geometry into a format suitable for a valid simulation run (Section 4.1); generating neutral and tool-specific BEPS files (Section 4.2); validating at the schema level (Section 4.3) and validating in the BEPS tools and post-processing (Section 4.4).

Most of the commonly available BEPS engines are based on one-dimensional heat transfer. In the context of building façades, the information required by these comparable BEPS tools is identical or almost identical. Notable considerations are as follows: (1) the order of points when defining surfaces and (2) the definition of zone-surface, surface-subsurface and surface to cross-section relationships [70]. The key parameters are:

- Surface name
- Parent surface name (relevant for doors and windows);
- Location of vertices using a standard coordinate system and;
- References to the cross-section type and the surface thermal properties.

Other information such as surface normals, view factors, and surface areas can be calculated from the information provided. An important difference between BEPS tools is the syntax through which the information is represented. Therefore, the conversion process would be almost identical for similar BEPS tools but with some minor syntax related variations. HVAC system and component representations are beyond the scope of this paper, if HVAC information was in a neutral file then very different conversion processes would be required for each BEPS tool. Furthermore the transformation process that uses the neutral file format must be consistent with the process presented by [16, 71].

4.1. Manual Parameter Input

Following the generation of a 3D geometric model for a given building, additional geometric and semantic information must be added to create input data for the BEPS tool. Geometric parameters include floor elevation and thickness of each floor slab and wall. While, these parameters could be automatically obtained by integrating laser scanning data from the exterior and interior of the building, such steps are out of the scope of this paper.

Semantic information includes the primary function of each floor (e.g. retail or office), the age of the building or year of the most recent major retrofit, and the materials of the windows, doors, walls, floors, and roof. Similarly, environmental information including usage profiles and equipment power densities must also be manually entered or can be selected from a template such as in Lagüela et al. [72]. The combination of this additional information with the processed point cloud is then used to create the wall, window, door, roof, and floor entities, as well as to determine the location of the windows and doors.

U-values are referenced by building element instances (wall, window or door) where each building element references a cross-section definition; for example Figure 6 contains a reference to a cross-section called "SinglePane-GlassWindow"). Each cross-section comprises a number of material layers that are stored in a defined order. The material properties for each material layer are available from public and proprietary sources or could be extracted from other scanning approaches such as that presented in Wang et al. [73]. U-values are calculated at run-time from the material layer properties of each cross-section.

Thermal zones or volumes of the buildings that are at the same environmental conditions are the fundamental building blocks of traditional BEPS simulations and must also be defined. The process starts with $\mathbf{Z} = \{z_i$, i = (0, . . .,N$\}$, the series of floor elevations, where z_0 and z_N are respectively the elevation of the ground and roof level. This implies that the number of zones (or storeys) within the building is N, and the lower and upper bounds of the zone i are z_i and $z'_i = z_i + 1$ - s_i, where s_i is the thickness of the floor slab i-th. Next, exterior surfaces of each zone are the exterior surfaces of the building vertical walls bounded by the lower and upper bounds of the zone, while the interior surfaces can be created by offsetting the exterior surface with the wall thickness. Thus, the geometric information for the zone involves interior surfaces and additional floor and ceiling or roof surfaces, respectively and openings (doors and windows) associated with the zone. The openings belonging to the Zone can be determined by comparing the vertices of the openings generated in a previous step to the lower and upper bounds of the zone. The opening is classified as a door, if any of its vertices connect to the ground level [39], otherwise, it is a window. Finally, for each zone, geometric and semantic information associated with environmental parameters are stored in the neutral file according the specification syntax required. At this point the BEPS data are in a neutral representation, the syntax of which must be adjusted to account for a specific BEPS tool (Section 4.2).

4.2. Neutral and Tool Specific BEPS File Generation

The file is created based on the outputs of the automated point cloud mapping and the manually added data. Figure 6 illustrates the representation of an example window in the standard ORACLE format for polygons, the neutral file format and the EnergyPlus file format. A one-to-one mapping of points and other properties is the key step in the conversion to the neutral file format. Please note that while the neutral file format closely aligns with the EnergyPlus file format, it is not identical.

Point Cloud Data Format

```
INSERT INTO Surface_With_Window VALUES(
  10,
  'polygon_with_hole',
  SDO_GEOMETRY(
        2003,  -- two-dimensional polygon
        NULL,
        NULL,
        SDO_ELEM_INFO_ARRAY(1,1003,1, 19,2003,1), -- polygon with hole
        SDO_ORDINATE_ARRAY(2,0, 14,0, 14,5, 2,5, 2,0,
              4,2, 7,2, 7,5, 4,5, 4,2)
   )
);
```

Neutral File Format	Comment	EnergyPlus IDF Format
FenestrationSurface,	!- Object Type	FenstrationSurface:Detailed
Window 1,	!- Object Type	Window 1,
Window,	!- Opening Type	Window,
SinglePaneGlassWindow,	!- Cross-section Name	SinglePaneGlassWindow,
Wall 1,	!- Parent Object Name	Wall 1,
Outside,	!- Ouside Boundary Condition	Outside,
AutoCalculate,	!- View Factor	AutoCalculate,
,	!- Shading Control Name	,
1,	!- Frame and Divider Name	1,
1,	!- Multiplier	1,
4,	!- Number of Vertices	4,
4.0, 0.0, 2.0,	!- Vertex 1 Coordinates	4.0, 0.0, 2.0,
7.0., 0.0, 2.0,	!- Vertex 2 Coordinates	7.0., 0.0, 2.0,
7.0., 0.0, 5.0,	!- Vertex 3 Coordinates	7.0., 0.0, 5.0,
4.0, 0.0, 5.0,	!- Vertex 4 Coordinates	4.0, 0.0, 5.0,

Legend	
Data from Point Cloud Process	(orange)
Manually Added Data	(green)

Figure 6: A window example for the three stages of data in the overall semi-automated process: point cloud format, the neutral file format and the EnergyPlus IDF format

The neutral file is of .txt format and does not adhere to the input format of any given BEPS tool. This approach follows the conventions adopted by seminal work in this area [16, 71].

The neutral file can be converted to a specific BEPS tool input format using a script or conversion tool. The design of this format allows for a one-to-one mapping of property instances between the neutral file (example provided in Figure 6) and the BEPS input file. The neutral file stores geometric information only and is not executable in any BEPS engine, the mandatory properties include:

- Surface name;
- Surface Type (wall, floor, ceiling or roof)
- Parent surface name (relevant for doors and windows);
- Outside boundary condition for the surface (set to outside for all façade surfaces) and;
- location of each vertex using a standard coordinate system;

This information is complemented by the manually inserted parameter values that include:

- Cross section name
- Zone name for parent surfaces
- Outside boundary condition
- Outside boundary condition object
- Sun exposure (optional)
- Wind exposure (optional)

4.3. Schema Level Validation

Model validation is then performed at two levels. The first is a routine validation against the target data model schema, while the second is within the modelling tool for verification of model suitability for compilation. These steps are discussed in detail below.

Validation of the BEPS inputs is specific to the targeted BEPS tool, for example EnergyPlus. The first rudimentary check is a comparison of the generated input file against the EnergyPlus schema file, called the Input Data Dictionary (IDD). This check is performed in a basic input tool called the IDF Editor, an interface for the EnergyPlus Input Data Format (IDF).

The schema level validation is a check that the input file is valid for a specific BEPS run, for example the contents of an XML file should adhere to the rules defined in a corresponding BEPS XSD schema. There are numerous XML or JSON tools available for this type of check, and such a check should be performed easily outside of a given simulation engine. Many of the established BEPS tools, such as EnergyPlus and DOE-2, are based on legacy system architectures that predate modern day best practice approaches for data management and do not have a formal schema. As a result, EnergyPlus does not provide this type of schema level validation prior to execution of a model. However, Simergy, an interface to EnergyPlus does. EnergyPlus is in the process of moving to a JSON schema and input files ([74]). Each BEPS tool should have its own rigorously defined schema.

4.4. Validation in BEPS Tool and post-processing

EnergyPlus is one of the most popular BEPS tools that engineers, architects, and researchers use to model energy and water usage in buildings and includes the most popular features and capabilities of the software packages BLAST and DOE-2.1E. As a result of the legacy code-base, key compilation and validation checks are performed during run-time, rather than beforehand. Various errors may then be generated, for example:

- Order of vertices when defining a surface;
- Surface normals pointing outward from the zone, as opposed to inward;
- Zones not enclosed;
- View factors;
- Incomplete data defined for a simulation run.

After the files are successfully uploaded to EnergyPlus, the requested output is a DXF file that is generated by the energy simulation tool for a final visualisation check. This technique has been applied in other relevant works in this area [16, 15]. The DXF file also describes floor and ceiling positions within the building.

5. Test case evaluation

5.1. Experimental tests

The objectives of the experiment were to evaluate the accuracy of the models generated by the proposed method and to determine to what extent such discrepancies impact downstream energy performance predictions. This was achieved through a comparison of (1) geometric measurements and (2) the annual energy consumption of BEPS models based on terrestrial laser scanning (TLS) data and independently measured CAD drawings. The proposed semi-automated process described in Sections 3 and 4 was applied to two buildings in Dublin, Ireland: No. 25 Westmoreland St. and No. 6 D'Olier St. These two buildings represent geometrically complex cases with different opening sizes and shapes. Both buildings have corresponding CAD drawings, which were used as the benchmark models when validating the building façade models. Building suitability was based on the time-period of construction. Each building has a different configuration of floors, windows, and doors (Figure 7a and Figure 8a). Actual geometric information for each building was based on a traditional survey and derived from drawings submitted to the Planning and Property Development Civic Offices of Dublin City Council (Table 2 and 3). Specific dimensions included length, height, and depth of the building, the dimensions of the building's openings, thickness of floor slabs and walls, and the floor elevation. The façade for No. 25 Westmoreland St. contains 5 floors, with 4 small doors (Door type I) and 1 large door (Door type II) on the bottom floor, 6 windows (Window type I) on the first floor, 5 small windows (Window type II) and 1 large window (Window type III) on the second floor, and 6 windows (Window type IV and V) on the fourth and fifth floors. Similarly, No. 6 D'Olier St. contains 5 floors, with a door (Door type I) and 3 large windows (Window type I and II) on the bottom floor, and 3 windows (Window type III, IV and V) on each subsequent floor.

Table 1: Size of the data sets for the two buildings

Building	Sampling data set		
	S20	S50	S75
No. 25 Westmoreland st.	353,848	71,155	35,468
No. 6 D'Olier st.	177,480	39,259	20,089

Point cloud data for these buildings were collected by a Trimble GS200 terrestrial laser scanner. Each building façade was scanned from different views to avoid omissions due to occlusions, and the data points were registered within RealWorkSurvey (RWS) V6.3. The source data set were mapped to the target based on pre-selected reference points, which are sharp features (e.g. a corner of the surface or window) although several methods could be used, for example surface matching algorithms [75]. The point cloud for the building of interest had to be manually separated from adjacent buildings within RWS V6.3, a current limitation of automatic extraction [76]. Next, the voxel-based region growing approach was employed to segment the data points of the building of interest using the approach and input parameters proposed by Vo et al. [59]. The results of segmentation allowed for elimination of irrelevant data points (e.g. internal objects such as furniture and ceilings). Thus, remaining data points describe vertical surfaces of the building and serve as input data for the proposed method, as defined in Section 3.1. For each building, three different sampling steps involving 20mm, 50mm and 75mm, were used to evaluate the influence of the sampling step on the geometric models. The TLS data of these buildings are shown in Table 1. Additionally, the selected terraced buildings are in an urban area, where it is extremely difficult to acquire data pertaining to side and back walls [39]. Therefore, in the process of 3D building generation based on TLS data, two assumptions were proposed: (1) the back wall is parallel to the street façade but has no openings and can be generated by offsetting the the facçade (not including openings) by the building depth, and (2) the side walls can be automatically generated by sweeping the side edges of the façade to the back wall [39]. Results of the building façade models from the proposed method are illustrated in Figure 7b, Figure 8b, and Table 2 and 3. Notably, since dimensions of each reconstructed opening in each storey of the façade differ, average dimensions of the reconstructed openings are shown in Tables 2 and 3.

The BEPS model for each building was automatically created by combining geometric building data generated from the proposed method in this paper with semantic information and environmental parameters. The geometry of the building was generated in a previous step, while the semantic information, such as the year of construction or the last major renovation for a given building was manually collected. The cross section types were assumed to be single course walls with interior plaster and single pane windows with wooden frames. Material layer properties of each cross-section were entered accordingly. The rudimentary modelling approach isolated the façade under investigation by representing these walls, windows and doors in details but all other surfaces as adiabatic, thus, focusing on the energy related impacts of the single façade alone. All zones used a constant temperature set point of 21°C for heating without a provision for cooling. Finally, Dublin, Ireland was set as the location, and both models used a simulation period of one year, for which publicly available climate data were used in the weather file.

Figure 7: (a) Westmoreland Street Façades and (b) Resulting building reconstruction from the proposed method

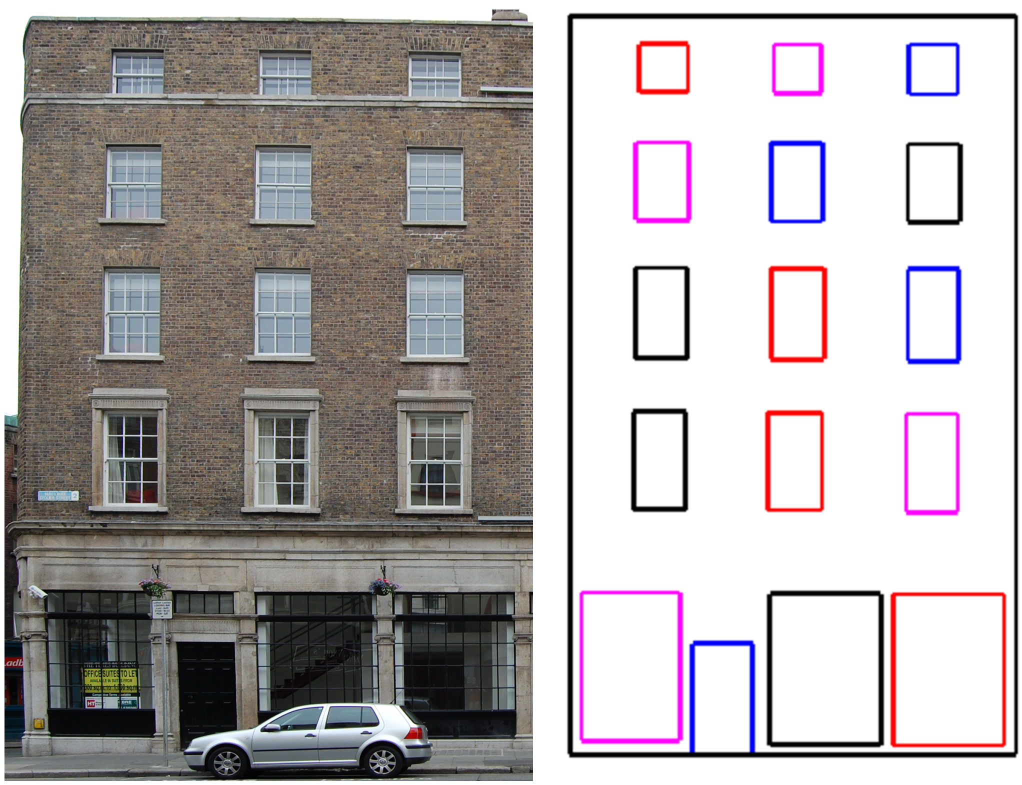

Figure 8: (a)D'Olier street façade and (b) Resulting building reconstruction from the proposed method, with evidence of occlusion

Table 2: Geometric information for No. 25 Westmoreland St.$^{(*)}$ denotes a manual BEPS entry for building models reconstructed from TLS data

		CAD	S20	S50	S75
Façade	Length (m)	19.36	19.31	19.27	19.24
	Height (m)	17.00	16.90	16.88	16.87
	Opening area (m^2)	96.17	96.71	98.02	99.18
	Depth (m)	11.03*			
	Wall thickness (m)	0.60*			
	Slab thickness (m)	0.296*			
	Number of storeys	5			
S1	Height: Flr.-Flr. (m)	4.25	4.25	4.25	4.25
	Door I (WxH) (m)	2.00x3.60	2.00x3.56	2.02x3.56	2.03x3.56
	Door II (WxH) (m)	4.90x3.60	4.92x3.56	4.93x3.56	4.95x3.56
	Tot. opening area (m^2)	46.44	45.97	46.27	46.51
	Tot. floor area (m^2)	213.56	213.00	212.53	212.24
	Tot. zone volume (m^3)	844.42	842.21	840.35	839.20
S2	Height: Flr.-Flr. (m)	3.61	3.61	3.61	3.61
	Window I (WxH) (m)	1.25x2.06	1.25x2.04	1.27x2.05	1.28x2.06
	Tot. opening area (m^2)	15.42	15.28	15.61	15.78
	Tot. floor area (m^2)	213.56	213.00	212.53	212.24
	Tot. zone volume (m^3)	710.94	709.08	707.52	706.55
S3	Height: Flr.-Flr. (m)	3.10	3.10	3.10	3.10
	Window II (WxH) (m)	1.25x1.65	1.25x1.66	1.26x1.67	1.27x1.69
	Window III (WxH) (m)	4.20x1.65	4.17x1.72	4.18x1.74	4.21x1.75
	Tot. opening area (m^2)	15.17	15.45	15.71	15.95
	Tot. floor area (m^2)	213.56	213.00	212.53	212.24
	Tot. zone volume (m^3)	594.55	593.00	591.69	590.88
S4	Height: Flr.-Flr. (m)	3.03	3.03	3.03	3.03
	Window IV (WxH) (m)	1.25x1.65	1.26x1.63	1.27x1.65	1.28x1.67
	Tot. opening area (m^2)	12.36	12.32	12.56	12.83
	Tot. floor area (m^2)	213.56	213.00	212.53	212.24
	Tot. zone volume (m^3)	583.87	582.35	581.06	580.27
S5	Height: Flr.-Flr. (m)	3.02	2.92	2.90	2.89
	Window V (WxH) (m)	1.25x0.90	1.26x1.03	1.27x1.03	1.24x1.10
	Tot. opening area (m^2)	6.78	7.69	7.87	8.11
	Tot. floor area (m^2)	213.56	213.00	212.53	212.24
	Tot. zone volume (m^3)	580.67	558.40	552.81	549.45

Table 3: Geometric information for No. 6 D'Olier St.(*) denotes a manual BEPS entry for building models reconstructed from TLS data

		CAD	S20	S50	S75
Façade	Length (m)	10.50	10.53	10.52	10.14
	Height (m)	17.46	17.43	17.42	17.42
	Opening area (m^2)	52.76	53.53	53.84	54.02
	Depth (m)	10.85(*)			
	Wall thickness (m)	0.60(*)			
	Slab thickness (m)	0.296(*)			
	Number of storeys	5	5	5	5
S1	Height: Flr.-Flr. (m)	5.29	5.29	5.29	5.29
	Door (WxH) (m)	1.30x2.65	1.39x2.62	1.40x2.62	1.42x2.62
	Window I (WxH) (m)	2.58x3.50	2.61x3.54	2.61x3.55	2.62x3.56
	Window II (WxH) (m)	2.26x3.50	2.31x3.49	2.33x3.51	2.33x3.50
	Tot. opening area (m^2)	25.97	26.51	26.67	26.79
	Tot. floor area (m^2)	113.92	114.27	212.53	212.24
	Tot. zone volume (m^3)	568.94	570.67	569.97	569.68
S2	Height: Flr.-Flr. (m)	3.50	3.50	3.50	3.50
	Window III (WxH) (m)	1.20x2.34	1.25x2.29	1.25x2.30	1.24x2.31
	Tot. opening area (m^2)	8.43	8.55	8.59	8.61
	Tot. floor area (m^2)	113.92	114.27	114.13	114.07
	Tot. zone volume (m^3)	365.02	366.13	365.67	365.49
S3	Height: Flr.-Flr. (m)	3.50	3.50	3.50	3.50
	Window IV (WxH) (m)	1.20x2.15	1.22x2.15	1.23x2.15	1.23x2.15
	Tot. opening area (m^2)	7.74	7.89	7.92	7.92
	Tot. floor area (m^2)	113.92	114.27	365.67	114.07
	Tot. zone volume (m^3)	365.02	366.13	552.81	365.49
S4	Height: Flr.-Flr. (m)	3.00	3.00	3.00	3.00
	Window V (WxH) (m)	1.20x1.85	1.22x1.83	1.23x1.84	1.23x1.84
	Tot. opening area (m^2)	6.66	6.70	6.75	6.78
	Tot. floor area (m^2)	113.92	114.27	308.61	114.07
	Tot. zone volume (m^3)	308.05	308.99	552.81	308.46
S5	Height: Flr.-Flr. (m)	2.17	2.14	2.13	2.13
	Window VI (WxH) (m)	1.20x1.10	1.14x1.14	1.14x1.15	1.14x1.15
	Tot. opening area (m^2)	3.96	3.88	3.91	3.92
	Tot. floor area (m^2)	113.92	114.27	114.13	114.07
	Tot. zone volume (m^3)	568.94	210.26	209.76	209.07

5.2. Results

The proposed method successfully generated 3D building models compatible with BEPS tools with only minimal manual intervention required. The models of the two buildings derived from the S50 data set are shown in Figure 9, while a summary of building geometries is presented in Table 2 and 3. Reconstructed building façade models with height and width values generally differed by under 1%, in terms of a relative error when compared to equivalent values from the reference data, a maximum absolute difference of 130 mm was found in the height of No. 25 Westmoreland St. Moreover, the proposed method also produced a building façade with an approximately 3% larger opening area than those in the reference data. The largest difference in terms of an opening area is 3.01 m^2 in No. 25 Westmoreland St. from the S75 data set. Similarly, dimensions of the reconstructed openings were overestimated by an maximum absolute average 57.2 mm [standard deviation (std) = 57.6 mm] for the height of No. 25 Westmoreland St.'s openings, and 46.9 mm (std = 28.9 mm) for the width of No. 6 D'Olier St.'s openings. Considering the discrepancy of openings' dimensions for each zone, the largest of which was found in zone 5 (top of the building). This is the maximum absolute difference of the window's height, and is 191mm for No. 25 Westmoreland St based on the S75 dataset. This in turn translates to an absolute difference of 1.33m^2 in terms of area. However, for other zones, in both buildings, differences in the opening area were mostly less than 0.5m^2. Finally, when considering the difference of the building models derived from CAD drawings and TLS data in term of a volume, the reconstructed building models differ around 1.4% (No. 25 Westmoreland st - CAD vs. S75) and 3.6% (No. 6 D'Olier st. - CAD vs. S75). Note that this comparison is based on height, length and depth of the building assumed as a block.

$$\begin{aligned} Relative_{\text{DifferenceEnergy}} = -0.0354 + 1.8386 * Difference_{\text{WallArea}} + \\ 1.0172 * Difference_{\text{OpeningArea}} \end{aligned} \tag{7}$$

Results of annual energy consumption of the buildings based on CAD and reconstructed models from TLS data are shown in Table 4. For No. 25 Westmoreland St., annual energy consumption from the CAD-based building was 89,142 kWh, which was greater than those from all generated model results within 1% for this surface of this value. A similar observation was found in No. 6 D'Olier St. The measured energy consumption based the

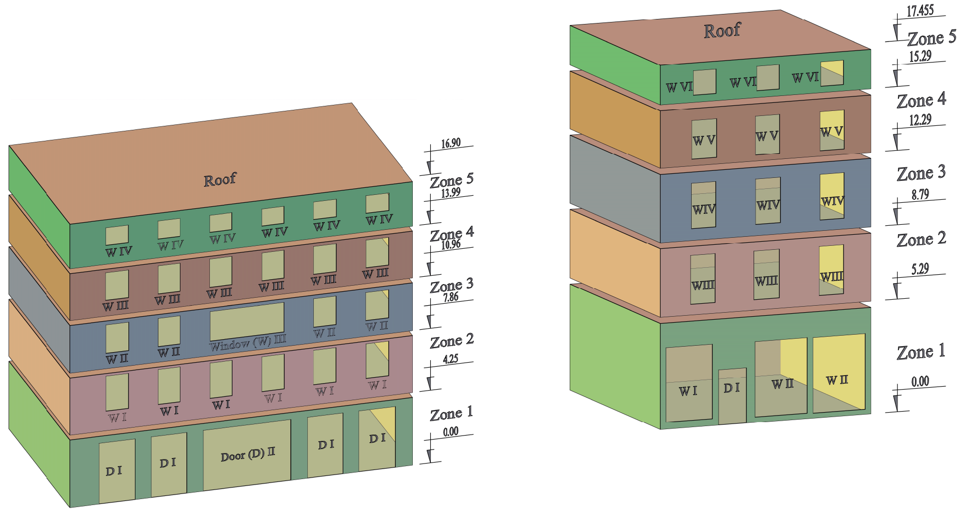

Figure 9: Illustration of building models for BEPS input (a) 25 Westmoreland st. and (b) 6 D'Olier st.

CAD model was 51,649 kWh, which is less than 1% smaller than those of all three generated models. This error is acceptable given that these are simplistic, indicative models, and in such cases, a model is considered calibrated if measured energy consumption values are within 10% of BEPS predictions on a monthly basis. The proposed semi-automated process could contribute inputs to a detailed model that could also include detailed HVAC and occupancy descriptions. In such cases, far more stringent calibration criteria would apply, which are beyond the scope of this paper.

Multi-variate linear regression was employed to explore the influence of geometric discrepancy on annual energy consumption. The goal of this work was to identify the relationship between the absolute difference in the building geometries (i.e. wall and opening area) and the relative difference of annual energy consumption (Table 5), where values from the CAD-based models were considered as the reference values. The analysis represented this relationship as in Equation 7 with $R^2 = 0.93$, as shown in Figure 10. This

Table 4: Annual building heating consumption (kWh)

Input data		CAD	S20	S50	S75
No. 25 Westmoreland st.					
Heating	Zone 1	20,966	20,886	20,861	20,847
	Zone 2	19,005	18,941	18,944	18,941
	Zone 3	16,800	16,786	16,783	16,791
	Zone 4	16,427	16,386	16,380	16,391
	Zone 5	15,944	15,505	15,389	15,333
	Total	**89,142**	**88,504**	**88,357**	**88,303**
No. 6 D'Olier st.					
Heating	Zone 1	16,086	16,219	16,225	16,230
	Zone 2	10,111	10,155	10,150	10,147
	Zone 3	10,261	10,308	10,297	10,294
	Zone 4	8,900	8,930	8,927	8,927
	Zone 5	6,291	6,211	6,200	6,183
	Total	**51,649**	**51,823**	**51,799**	**51,781**

implies that the differences in wall and opening areas significantly influenced the change of the annual energy consumption.

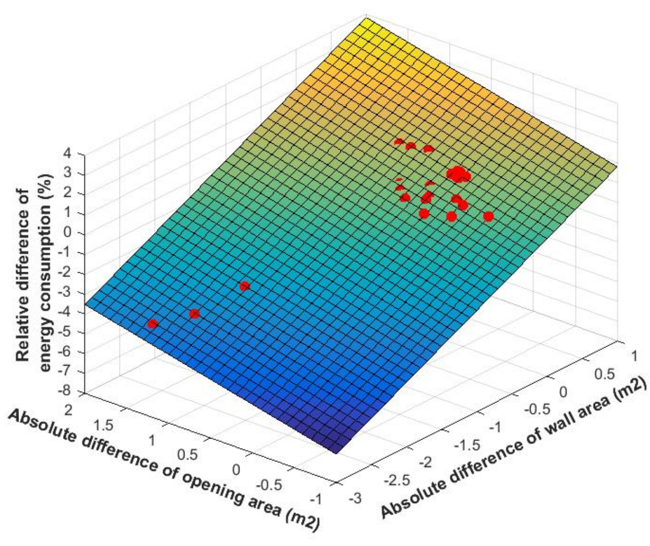

Figure 10: Relationship between building geometry and energy consumptions

Table 5: Absolute difference of geometry and relative difference of energy consumption

		No. 25 Westmoreland st.			No. 6 D'Olier st.		
		CAD vs. S20	CAD vs. S50	CAD vs. S75	CAD vs. S20	CAD vs. S50	CAD vs. S75
Wall area (m^2)	Zone 1	-0.20	-0.37	-0.47	0.16	0.09	0.07
	Zone 2	-0.17	-0.31	-0.40	0.10	0.06	0.05
	Zone 3	-0.14	-0.26	-0.33	0.10	0.06	0.05
	Zone 4	-0.14	-0.25	-0.33	0.09	0.05	0.04
	Zone 5	-2.02	-2.53	-2.83	-0.24	-0.29	-0.35
Openings' area (m^2)	Zone 1	-0.47	-0.17	0.07	0.54	0.70	0.82
	Zone 2	-0.14	0.19	0.36	0.12	0.16	0.18
	Zone 3	0.28	0.54	0.78	0.15	0.18	0.18
	Zone 4	-0.04	0.20	0.47	0.04	0.09	0.12
	Zone 5	0.91	1.09	1.33	-0.08	-0.05	-0.04
Heating (%)	Zone 1	-0.38	-0.50	-0.57	0.83	0.86	0.90
	Zone 2	-0.34	-0.32	-0.34	0.44	0.38	0.36
	Zone 3	-0.08	-0.10	-0.05	0.46	0.35	0.32
	Zone 4	-0.25	-0.29	-0.22	0.34	0.31	0.31
	Zone 5	-2.75	-3.48	-3.83	-1.28	-1.46	-1.72

5.3. Discussion

This paper introduces a semi-automated, seamless, scalable, and robust method for reconstructing façades of 3D building models without requirements for any third party software or a priori information. The proposed method is suitable for generating building models with features comprising linear boundaries; it cannot yet account for building components with non-linear (i.e. curve or circle) boundaries. Such functionality would require the introduction of additional algorithms or unsupervised learning techniques to classify component boundaries as linear and non-linear, with an accompanying fitting procedure to determine the boundary line of best fit based on the root mean square error of the fitting.

The proposed method was successful in the construction of 3D building models for two building façades from different sampling steps. Relative errors of the façades' and openings' dimensions are less than 1% and 3%, respectively, while the maximum average relative errors of opening areas are 6.4% for a data set of S75 from 25 Westmoreland St. and and 2.6% for 6 D'Olier St. This implies that the quality of the building models derived from the proposed method is better than a previous work done by Díaz-Vilariño et. al. [40], which generated the openings with an average relative error of 11.7%. Moreover, although the sampling step is up to 75 mm (Table 1), the RMSEs of the façade dimensions and its openings are respectively 125.1 mm and 61.5 mm for 25 Westmoreland st., and 27.3 mm and 46.1 mm for 6 D'Olier St. (Figure 11a & b). Those errors are generally less than the sampling step, which is consistent with the conclusions of Tang et al. [68]. In such cases, edge losses due to spatial discontinuities of a point cloud arise when the laser beam hits the edge of solid object and this can be up to several centimetres. Moreover, it also noted that the proposed method gave errors of the same order when compared to previous research: an average error for window size of 5.39cm (std = 5.70cm) [44], an RMSE of the walls' vertices about 4.8cm [46] and 7.4cm [43], a maximum distance error for the walls' vertices in a range from $4.29 \pm 0.53cm$ to $45.74 \pm 5.52cm$. Moreover, when considering an error in terms of an area, results from the proposed method are also comparable with a work of Tamke et al. [47] with an error about 9.8% or Quintana et al. [49] with an error of 1.7% regarding to detected openings.

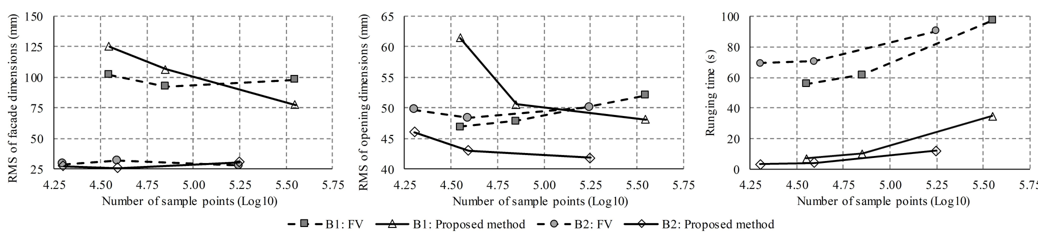

Figure 11: Comparing performance of the proposed method vs. the façade method developed by [61]: a) RMSE of façade's dimensions, b) RMSE of openings' dimensions, c) Running time

In addition, performance of the proposed method in terms of quality of the building models and execution time was compared to that of the façade voxel (FV) method developed by Truong-Hong and Laefer [61], an automatic method for 3D building reconstruction. Both algorithms were implemented in Matlab 2016a environment and run on a HP EliteBook 2570p with Intel (R) Core i7-3520M, CPU @2.9GHz, 16Gb RAM, OS Window 10. The geometric building models from the algorithms were compared to the CAD models to identify geometric discrepancies. Results showed that the the proposed method can generate the building models with the same accuracy level to the building models from FV method. However, the proposed method reconstructed successfully 25 Westmoreland St. - with 28 openings - with an input data size about 353k points in 35 seconds. This makes this method faster than the FV method by about 5.5 times for 25 Westmoreland St., and 14.8 times for 6 D'Olier St. (Figure 11c).

The method introduced in this paper is limited to reconstructing building façades and their openings, particularly the windows/doors covered by low reflectance materials and/or located with a slight recession from exterior surface of the wall. In the case of solid, wholly openings with no recessed portions, additional attributes of the point cloud, known as the laser backscatter intensity or red-green-blue colour of the point cloud could be used to establish the threshold that distinguishes between the points of the wall and those of the window/door areas.

Generated BEPS models from the proposed work flow contain accurate representations of such façades but do not yet include detailed interior representations of the building. A higher LoD for the building, e.g. LoD 4 offers significant potential for comprehensive representation of the building geometry which can be transformed into BEPS models. This still presents a significant challenge in terms of data acquisition and processing. A complete representation of the building could be achieved by integrating data from other sources, for example: aerial laser scanning or unmanned vehicle aerial based laser scanning/images, which can provide point clouds for building roofs and other parts that remain inaccessible to TLS from the ground.

Although the TLS has often been used to capture internal building elements [19], the method requires significant labour on site because the complexity of the building and obstructions from furniture necessitates a large number of scan stations. In addition, it requires huge effort to register data points from the large number of the scan stations and to clean irrelevant data points. To reduce such overheads, a possible solution is to use a robot with a scanner or a backpack scanner [23]. The advantage of these units is to reduce time for setting up scan stations, which takes a large portion of operating time for today's modern scanners, for target acquisition, and office labour for data registration.

In terms of data processing, the data set may contain up to a billion points and be gigabytes in size. Such data will require new, efficient indexing and management. Additionally, new, efficient and robust methods should be developed to extract and reconstruct internal walls, floors, ceilings and other building components. Existing methods are limited to extracting and reconstructing planar objects or separate rooms. For example, Okorn et al.

[77] succeeded in extracting flat floors and ceilings from a point cloud, while Turner et. al. (2015) generated models for separate rooms [78]. Further information (e.g. the thickness of the walls or floors, the types of building component material) should ideally also be automatically determined from sensing data, to improve the automation of the pipeline transforming sensed data into a BEPS model.

Although the sensitivity analysis performed in this paper shows that rudimentary geometric models derived from a point cloud differed by approximately 1% compared to equivalent models from reference data, it is clear that such discrepancies in geometry do not significantly impact estimations of building energy usage. Similar analysis needs to be performed and validated in a more comprehensive evaluation that considers a complete representation of building geometries. Such experimentation would help to remove uncertainty with respect to the contribution of building geometry to the overall "performance gap" issue in buildings.

6. Conclusions and Future Work

The generation of input data for energy simulation purposes has been a time-consuming and laborious task, particularly the collection and processing of building geometry information. Laser scanning data provides highly detailed topographic information for a building, which can provide an opportunity to generate 3D building models quickly and accurately in a automated fashion. The models can be used as a basis for BEPS model inputs by adding further manual inputs not just for one-off projects but as a scalable solution that is applicable to the majority of the existing urban building stock.

This paper describes a semi-automated process whereby point cloud data captured by TLS is automatically transformed into usable geometric format for a specific BEPS tool, EnergyPlus. The semi-automated process subsequently requires manual input of basic semantic information for a given building. The work demonstrates a worthwhile and potentially scalable solution applicable to existing buildings. In this process, utmost care must be taken when scanning multiple building storeys from a fixed horizontal plane as scanning inaccuracies can have a downstream impact on building energy performance prediction.

BEPS has an important role to the play in the renovation of the existing building stock by enabling the rapid creation of simulation models in a semi-automated manner. If the costs of creating these models are significantly reduced, owners and operators will be better able to cost-effectively use simulation tools as standard practice for retrofit scenario modelling.

Future work in this area includes the extension of this technique to capture an entire building (exterior and interior objects) and to generate more complicated structures and building elements such as roofs, free-form surfaces, internal objects (e.g. ceiling, internal walls), shading elements, façades of non-terraced buildings, and skyscrapers. The integration of terrestrial and aerial point data clouds may also benefit 3D building models with LoD 4 by facilitating the coupling of exterior and interior building models. Finally, the transformation of point clouds to BIM and GIS based formats offers the potential for simulation at neighbourhood, district, and city scales.

7. Acknowledgements

This work was supported by a Marie Curie FP7 Integration Grant within the 7th European Union Framework Programme project title SuPerB, project number 631617. The third and last authors are graceful the generous support of the European Commission through FP7 ERC Consolidator grant, "RETURN: Rethinking Tunnelling for Urban Neighbourhoods"), ERC StG 2012-307836-RETURN. The authors would like Cathal Hoare for proof reading the final manuscript.

8. References

[1] T. A. Reddy, I. Maor, C. Panjapornpon, Calibrating detailed building energy simulation programs with measured data—part i: General methodology (rp-1051), Hvac&R Research 13 (2) (2007) 221–241. doi:10.1080/10789669.2007.10390952.

[2] C. Turner, Frankel, Energy Performance of LEED for New Construction Buildings, Final Final Version, New Buildings Institute, PO Box 2349 White Salmon, WA 98672 509-493-4468 1331 Washington Street Vancouver, WA 98660 (Mar. 2008).
URL https://www.usgbc.org/drupal/legacy/usgbc/docs/Archive/General/Docs3930.pdf

[3] J. H. Scofield, Do LEED-certified buildings save energy? Not really..., Energy and Buildings 41 (12) (2009) 1386 – 1390.

doi:10.1016/j.enbuild.2009.08.006.
URL http://www.sciencedirect.com/science/article/pii/S037877880900187X

[4] P. de Wilde, R. Jones, The building energy performance gap: Up close and personal, in: CIBSE ASHRAE Technical Symposium: Moving to a new world of building systems performance, 2014, pp. 1–12.
URL https://www.cibse.org/technical-symposium-2019/past-papers-case-studies-archive/2014

[5] A. C. Menezes, A. Cripps, D. Bouchlaghem, R. Buswell, Predicted vs. actual energy performance of non-domestic buildings: Using post-occupancy evaluation data to reduce the performance gap, Energy Solutions for a Sustainable World - Proceedings of the Third International Conference on Applied Energy, May 16-18, 2011 - Perugia, Italy 97 (0) (2012) 355–364. doi:10.1016/j.apenergy.2011.11.075.
URL http://www.sciencedirect.com/science/article/pii/S0306261911007811

[6] J. O'Donnell, M. Keane, E. Morrissey, V. Bazjanac, Scenario modelling: A holistic environmental and energy management method for building operation optimisation, Energy and Buildings 62 (2013) 146–157. doi:10.1016/j.enbuild.2012.10.060.
URL http://www.sciencedirect.com/science/article/pii/S0378778813001345

[7] D. Coakley, E. Corry, M. Keane, Validation of Simulated Thermal Comfort using a Calibrated Building Energy Simulation (BES) model in the context of Building Performance Evaluation & Optimisation, in: 13th annual International Conference for Enhanced Building Operations (ICEBO), Energy Systems Laboratory, Texas A&M University (http://www.tamu.edu), 2013, pp. 1–12.
URL http://hdl.handle.net/1969.1/151416

[8] I. Z. Bribián, A. A. Usón, O. S. Cardaño, A. Munar, Development of European Ecolabel and Green Public Procurement Criteria for Office Buildings JRC IPTS Draft Report, Tech. rep., Joint Research Center European Commission, Seville, Spain (Jun. 2011).
URL http://susproc.jrc.ec.europa.eu/buildings/docs/product%20definition%20and%20scope.pdf

[9] P. de Wilde, The gap between predicted and measured energy performance of buildings: A framework for investigation, Automation in Construction 41 (1) (2014) 40–49. doi:10.1016/j.autcon.2014.02.009.
URL http://www.sciencedirect.com/science/article/pii/S092658051400034X

[10] Y. K. Cho, Y. Ham, M. Golpavar-Fard, 3D as-is building energy modeling and diagnostics: A review of the state-of-the-art, Advanced Engineering Informatics 29 (2) (2015) 184 – 195, infrastructure Computer Vision. doi:10.1016/j.aei.2015.03.004.
URL http://www.sciencedirect.com/science/article/pii/S1474034615000312

[11] J. Jung, S. Hong, S. Jeong, S. Kim, H. Cho, S. Hong, J. Heo, Productive modeling for development of as-built BIM of existing indoor structures, Automation in Construction 42 (0) (2014) 68 – 77. doi:10.1016/j.autcon.2014.02.021.
URL http://www.sciencedirect.com/science/article/pii/S0926580514000466

[12] F. Bosché, M. Ahmed, Y. Turkan, C. T. Haas, R. Haas, The value of integrating Scan-to-BIM and Scan-vs-BIM techniques for construction monitoring using laser scanning and BIM: The case of cylindrical {MEP} components, Automation in Construction 49 Part B (1) (2015) 201–213. doi:10.1016/j.autcon.2014.05.014.
URL http://www.sciencedirect.com/science/article/pii/S0926580514001319

[13] C. Früh, A. Zakhor, An Automated Method for Large-Scale, Ground-Based City Model Acquisition, International Journal of Computer Vision 60 (1) (2004) 5–24. doi:10.1023/B:VISI.0000027787.82851.b6.
URL http://dx.doi.org/10.1023/B%3AVISI.0000027787.82851.b6

[14] V. Bazjanac, Acquisition of Building Geometry in the Simulation of Energy Performance, in: 7th International IBPSA Conference Building Simulation 2001, IBPSA ISSN 2522-2708, Rio de Janeiro, Brazil, 2001, pp. 305–312.
URL http://www.ibpsa.org/proceedings/BS2001/BS01_0305_312.pdf

[15] J. O'Donnell, T. Maile, C. Rose, N. Mrazović, E. Morrissey, C. Regnier, K. Parrish, V. Bazjanac, Transforming BIM to BEM: Generation of Building Geometry for the NASA Ames Sustainability Base BIM, Tech. Rep. LBNL-6033E, LBNL (2013).
URL `http://eetd.lbl.gov/node/51468`

[16] C. M. Rose, V. Bazjanac, An algorithm to generate space boundaries for building energy simulation, Engineering with Computers 31 (2015) 271–280. `doi:10.1007/s00366-013-0347-5`.
URL `http://link.springer.com/10.1007/s00366-013-0347-5`

[17] C. van Treeck, E. Rank, Dimensional reduction of 3d building models using graph theory and its application in building energy simulation, Engineering with Computers 23 (2) (2007) 109–122. `doi:10.1007/s00366-006-0053-7`.
URL `http://link.springer.com/article/10.1007/s00366-006-0053-7`

[18] T. L. Garwood, B. R. Hughes, D. O'Connor, J. K. Calautit, M. R. Oates, T. Hodgson, A framework for producing gbXML building geometry from Point Clouds for accurate and efficient Building Energy Modelling, Applied Energy 224 (2018) 527–537. `doi:10.1016/j.apenergy.2018.04.046`.
URL `http://www.sciencedirect.com/science/article/pii/S0306261918306044`

[19] T. L. Garwood, B. R. Hughes, D. O'Connor, J. K. Calautit, M. R. Oates, T. Hodgson, Geometry Extraction for High Resolution Building Energy Modelling Applications from Point Cloud Data: A Case Study of a Factory Facility, Energy Procedia 142 (2017) 1805–1810. `doi:10.1016/j.egypro.2017.12.567`.
URL `http://www.sciencedirect.com/science/article/pii/S1876610217363233`

[20] A. Budroni, J. Böhm, Toward automatic reconstruction of interiors from laser data, in: Proceedings of Virtual Reconstruction and Visualization of Complex Architectures (3D-Arch), ISPRS, p. 7.
URL `https://www.isprs.org/proceedings/XXXVIII/5-W1/pdf/budroni_boehm.pdf`

[21] E. Valero, A. Adán, C. Cerrada, Automatic method for building indoor boundary models from dense point clouds collected by laser scanners, Sensors 12 (12) (2012) 16099–16115. doi:10.3390/s121216099.
URL http://www.mdpi.com/1424-8220/12/12/16099

[22] V. Sanchez, A. Zakhor, Planar 3D modeling of building interiors from point cloud data, in: 19th IEEE International Conference on Image Processing, 2012, pp. 1777–1780. doi:10.1109/ICIP.2012.6467225.

[23] W. Shi, W. Ahmed, N. Li, W. Fan, H. Xiang, M. Wang, Semantic Geometric Modelling of Unstructured Indoor Point Cloud, ISPRS International Journal of Geo-Information 8 (1) (2019) 9. doi:10.3390/ijgi8010009.
URL https://www.mdpi.com/2220-9964/8/1/9

[24] V. Bazjanac, T. Maile, C. Nytsch-Geusen, Generation of building geometry for energy performance simulation using Modelica, in: BauSim Conference, Dresden, Germany, 2016, pp. 361–368.
URL http://www.ibpsa.org/proceedings/bausimPapers/2016/D-01-1.pdf

[25] Y. Ham, M. Golparvar-Fard, An automated vision-based method for rapid 3d energy performance modeling of existing buildings using thermal and digital imagery, Advanced Engineering Informatics 27 (3) (2013) 395–409. doi:10.1016/j.aei.2013.03.005.
URL http://www.sciencedirect.com/science/article/pii/S147403461300027X

[26] Technical University Berlin, Energy Atlas Berlin, [Accessed 2-10-2018] (2015).
URL http://energyatlas.energie.tu-berlin.de/

[27] L. Madrazo, SEMANCO, [Accessed 2-10-2018] (2015).
URL http://www.semanco-project.eu/

[28] S. L. López, J. C. García, J. M. Sánchez, D. R. Bernárdez, H. L. Cimadevila, Thermographic mobile mapping of urban environment for lighting and energy studies, Journal of Daylighting 1 (1) (2014) 8–15. doi:10.15627/jd.2014.2.

[29] K. Maragkogiannis, D. Kolokotsa, E. Maravelakis, A. Konstantaras, Combining terrestrial laser scanning and computational fluid dynamics for the study of the urban thermal environment, Sustainable Cities and Society 13 (Supplement C) (2014) 207 – 216. doi:10.1016/j.scs.2013.12.002.
URL http://www.sciencedirect.com/science/article/pii/S2210670713000851

[30] S. Lagüela, J. Martínez, J. Armesto, P. Arias, Energy efficiency studies through 3D laser scanning and thermographic technologies, Energy and Buildings 43 (6) (2011) 1216 – 1221. doi:https://doi.org/10.1016/j.enbuild.2010.12.031.
URL http://www.sciencedirect.com/science/article/pii/S0378778811000041

[31] D. González-Aguilera, S. Lagüela, P. Rodríguez-Gonzálvez, D. Hernández-López, Image-based thermographic modeling for assessing energy efficiency of buildings façades, Energy and Buildings 65 (Supplement C) (2013) 29 – 36. doi:10.1016/j.enbuild.2013.05.040.
URL http://www.sciencedirect.com/science/article/pii/S0378778813003289

[32] S. Lagüela, L. Díaz-Vilariño, J. Martínez, J. Armesto, Automatic thermographic and RGB texture of as-built BIM for energy rehabilitation purposes, Automation in Construction 31 (0) (2013) 230 – 240. doi:10.1016/j.autcon.2012.12.013.
URL http://www.sciencedirect.com/science/article/pii/S092658051200252X

[33] D. Borrmann, A. Nüchter, M. Đakulović, I. Maurović, I. Petrović, D. Osmanković, J. Velagić, A mobile robot based system for fully automated thermal 3D mapping, Advanced Engineering Informatics 28 (4) (2014) 425 – 440. doi:10.1016/j.aei.2014.06.002.
URL http://www.sciencedirect.com/science/article/pii/S1474034614000408

[34] Y. Cho, C. Wang, 3D thermal modeling for existing buildings using hybrid LIDAR system, in: Computing in Civil Engineering (2011), Miami, Florida, pp. 552–559. doi:10.1061/41182(416)68.

URL https://ascelibrary.org/doi/abs/10.1061/41182%28416%2968

[35] F. Moran, T. Blight, S. Natarajan, A. Shea, The use of passive house planning package to reduce energy use and co_2 emissions in historic dwellings, Energy and Buildings 75 (Supplement C) (2014) 216 – 227. doi:10.1016/j.enbuild.2013.12.043.
URL http://www.sciencedirect.com/science/article/pii/S0378778813008608

[36] M. Morelli, L. Rønby, S. E. Mikkelsen, M. G. Minzari, T. Kildemoes, H. M. Tommerup, Energy retrofitting of a typical old danish multifamily building to a "nearly-zero" energy building based on experiences from a test apartment, Energy and Buildings 54 (Supplement C) (2012) 395 – 406. doi:https://doi.org/10.1016/j.enbuild.2012.07.046.
URL http://www.sciencedirect.com/science/article/pii/S0378778812004021

[37] Y. Ham, M. Golparvar-Fard, Mapping actual thermal properties to building elements in gbXML-based BIM for reliable building energy performance modeling, Automation in Construction 49, Part B (2015) 214–224. doi:10.1016/j.autcon.2014.07.009.
URL http://www.sciencedirect.com/science/article/pii/S0926580514001605

[38] L. Truong-Hong, D. F. Laefer, T. Hinks, H. Carr, Flying Voxel Method with Delaunay Triangulation Criterion for Façades/Feature Detection for Computation, Journal of Computing in Civil Engineering 26 (6) (2012) 691–707. doi:10.1061/(ASCE)CP.1943-5487.0000188.
URL http://ascelibrary.org/doi/abs/10.1061/%28ASCE%29CP.1943-5487.0000188

[39] S. Pu, G. Vosselman, Knowledge based reconstruction of building models from terrestrial laser scanning data, ISPRS Journal of Photogrammetry and Remote Sensing 64 (6) (2009) 575–584. doi:10.1016/j.isprsjprs.2009.04.001.
URL https://www.sciencedirect.com/science/article/abs/pii/S0924271609000501

[40] L. Díaz-Vilariño, S. Lagüela, J. Armesto, P. Arias, Indoor daylight simulation performed on automatically generated as-built 3D models, Energy and Buildings 68 (2014) 54–62. doi:10.1016/j.enbuild.2013.02.064.
URL https://www.sciencedirect.com/science/article/pii/S0378778813006038

[41] S. M. Iman Zolanvari, D. F. Laefer, Slicing Method for curved façade and window extraction from point clouds, ISPRS Journal of Photogrammetry and Remote Sensing 119 (2016) 334–346. doi:10.1016/j.isprsjprs.2016.06.011.
URL http://www.sciencedirect.com/science/article/pii/S0924271616301228

[42] J. Li, B. Xiong, F. Biljecki, G. Schrotter, A sliding window method for detecting corners of openings from terrestrial lidar data, ISPRS - International Archives of the Photogrammetry, Remote Sensing and Spatial Information Sciences XLII-4/W10 (2018) 97–103. doi:10.5194/isprs-archives-XLII-4-W10-97-2018.
URL https://www.int-arch-photogramm-remote-sens-spatial-inf-sci.net/XLII-4-W10/97/2018/

[43] J. Jung, C. Stachniss, S. Ju, J. Heo, Automated 3d volumetric reconstruction of multiple-room building interiors for as-built BIM, Advanced Engineering Informatics 38 (2018) 811–825. doi:10.1016/j.aei.2018.10.007.
URL http://www.sciencedirect.com/science/article/pii/S1474034618300600

[44] A. Adan, D. Huber, 3D reconstruction of interior wall surfaces under occlusion and clutter, in: 2011 International Conference on 3D Imaging, Modeling, Processing, Visualization and Transmission, IEEE, 2011, pp. 275–281. doi:10.1109/3DIMPVT.2011.42.

[45] C. Wang, Y. K. Cho, Automatic as-is 3D building models creation from unorganized point clouds, in: Construction Research Congress 2014, 2014, pp. 917–924. doi:10.1061/9780784413517.094.
URL https://ascelibrary.org/doi/abs/10.1061/9780784413517.094

[46] J. Jung, S. Hong, S. Yoon, J. Kim, J. Heo, Automated 3d wireframe modeling of indoor structures from point clouds using constrained least-squares adjustment for as-built bim, Journal of Computing in Civil Engineering 30 (4) (2016) 04015074. arXiv:https://ascelibrary.org/doi/pdf/10.1061/\%28ASCE\%29CP.1943-5487.0000556, doi:10.1061/(ASCE)CP.1943-5487.0000556.
URL https://ascelibrary.org/doi/abs/10.1061/%28ASCE%29CP.1943-5487.0000556

[47] M. Tamke, H. L. Evers, M. Zwierzycki, R. Wessel, S. Ochmann, R. Vock, R. Klein, An automated approach to the generation of structured building information models from unstructured 3d point cloud scans, in: Proceedings of IASS Annual Symposia, Vol. 2016, International Association for Shell and Spatial Structures (IASS), 2016, pp. 1–10.
URL https://adk.elsevierpure.com/en/publications/an-automated-approach-to-the-generation-of-structured-building-in

[48] S. Ochmann, R. Vock, R. Wessel, R. Klein, Automatic reconstruction of parametric building models from indoor point clouds, Computers & Graphics 54 (2016) 94–103. doi:10.1016/j.cag.2015.07.008.
URL http://www.sciencedirect.com/science/article/pii/S0097849315001119

[49] B. Quintana, S. A. Prieto, A. Adán, F. Bosché, Door detection in 3d coloured point clouds of indoor environments, Automation in Construction 85 (2018) 146–166. doi:10.1016/j.autcon.2017.10.016.
URL http://www.sciencedirect.com/science/article/pii/S0926580516302400

[50] B. Staats, A. Diakité, R. Voûte, S. Zlatanova, Detection of doors in a voxel model, derived from a point cloud and its scanner trajectory, to improve the segmentation of the walkable space, International Journal of Urban Sciences (2018) 1–22doi:10.1080/12265934.2018.1553685.
URL https://doi.org/10.1080/12265934.2018.1553685

[51] L. Li, F. Su, F. Yang, H. Zhu, D. Li, X. Zuo, F. Li, Y. Liu, S. Ying, Reconstruction of Three-Dimensional (3d) Indoor Interiors with Multiple Stories via Comprehensive Segmentation, Remote Sensing 10 (8) (2018)

1281. doi:10.3390/rs10081281.
URL https://www.mdpi.com/2072-4292/10/8/1281

[52] H. Tran, K. Khoshelham, A. Kealy, L. Díaz-Vilariño, Shape grammar approach to 3d modeling of indoor environments using point clouds, Journal of Computing in Civil Engineering 33 (1) (2018) 04018055. doi:10.1061/(ASCE)CP.1943-5487.0000800.
URL https://ascelibrary.org/doi/10.1061/%28ASCE%29CP.1943-5487.0000800

[53] C. Wang, S. Hou, C. Wen, Z. Gong, Q. Li, X. Sun, J. Li, Semantic line framework-based indoor building modeling using backpacked laser scanning point cloud, ISPRS Journal of Photogrammetry and Remote Sensing 143 (2018) 150–166. doi:10.1016/j.isprsjprs.2018.03.025.
URL http://www.sciencedirect.com/science/article/pii/S092427161830090X

[54] M. Neuhausen, M. König, Automatic window detection in facade images, Automation in Construction 96 (2018) 527 – 539. doi:https://doi.org/10.1016/j.autcon.2018.10.007.
URL http://www.sciencedirect.com/science/article/pii/S092658051830551X

[55] G. Gröger, T. Kolbe, C. Nagel, K. Hafele, OpenGIS City Geography Markup Language (CityGML) Encoding Standard (OGC 12-019). Version 2.0.0. OGC 12-019., last accessed 2014-11-03 (2014).
URL http://www.opengeospatial.org/standards/citygml

[56] Trimble Navigation Limited, RealWork Survey Advanced, last accessed 2014-11-03 (2014).
URL https://geospatial.trimble.com/products-and-solutions/trimble-realworks

[57] T. Rabbani, F. van den Heuvel, G. Vosselman, Segmentation of point clouds using smoothness constraints, in: H. Maas, D. Schneider (Eds.), ISPRS 2006 : Proceedings of the ISPRS commission V symposium Vol. 35, part 6 : image engineering and vision metrology, Dresden, Germany 25-27 September 2006, Vol. 35, ISSN 1682-1750, International Society for Photogrammetry and Remote Sensing (ISPRS), 2006, pp. 248–253.

[58] R. Schnabel, R. Wahl, R. Klein, Efficient ransac for point-cloud shape detection, Computer Graphics Forum 26 (2) (2007) 214–226.
URL http://cg.cs.uni-bonn.de/en/publications/paper-details/schnabel-2007-efficient/

[59] A.-V. Vo, L. Truong-Hong, D. F. Laefer, M. Bertolotto, Octree-based region growing for point cloud segmentation, {ISPRS} Journal of Photogrammetry and Remote Sensing 104 (2015) 88 – 100. doi:http://dx.doi.org/10.1016/j.isprsjprs.2015.01.011.
URL http://www.sciencedirect.com/science/article/pii/S0924271615000283

[60] H. Hoppe, T. DeRose, T. Duchamp, J. McDonald, W. Stuetzle, Surface reconstruction from unorganized points, SIGGRAPH Comput. Graph. 26 (2) (1992) 71–78. doi:10.1145/142920.134011.
URL http://doi.acm.org/10.1145/142920.134011

[61] L. Truong-Hong, D. F. Laefer, Octree-based, automatic building façade generation from LiDAR data, Computer-Aided Design 53 (2014) 46–61. doi:10.1016/j.cad.2014.03.001.

[62] N. Ripperda, Determination of façade attributes for façade reconstruction, International Archives of Photogrammetry, Remote Sensing and Spatial Information Sciences 37 (B3.a) (2008) 285–290.
URL http://www.isprs.org/proceedings/XXXVII/congress/3_pdf/44.pdf

[63] S. Becker, N. Haala, Refinement of building fassades by integrated processing of LIDAR and image data, International Archives of Photogrammetry, Remote Sensing and Spatial Information Science 36 (2007) 7–12.
URL http://www.ifp.uni-stuttgart.de/publications/2007/becker_haala_pia07.pdf

[64] S. Pu, G. Vosselman, Extracting windows from terrestrial laser scanning, in: ISPRS Workshop on Laser Scanning and SilviLaser, Espoo, Finland, 2007, pp. 320–5.
URL https://foto.aalto.fi/ls2007/

[65] G. H. Bendels, R. Schnabel, R. Klein, Detecting holes in point set surfaces, in: V. Skala (Ed.), The 14^{th} International Conference in Central Europe on Computer Graphics, Visualization and Computer Vision 2006 (WSCG 2006), Vol. 14, UNION Agency-Science Press, ISSN 1213-6972, 2006.
URL `http://cg.cs.uni-bonn.de/aigaion2root/attachments/bendels-2006-detecting.pdf`

[66] L. Truong-Hong, D. F. Laefer, T. Hinks, H. Carr, Combining an angle criterion with voxelization and the flying voxel method in reconstructing building models from LiDAR data, Computer-Aided Civil and Infrastructure Engineering 28 (2) (2013) 112–129. `doi:10.1111/j.1467-8667.2012.00761.x`.

[67] F. Pighin, J. Lewis, Siggraph 2007 course notes Practical Least-Squares for Computer Graphics, http://graphics.stanford.edu/ jplewis/lscourse/ls.pdf (2007).

[68] P. Tang, B. Akinci, D. Huber, Quantification of edge loss of laser scanned data at spatial discontinuities, Automation in Construction 18 (8) (2009) 1070–1083. `doi:10.1016/j.autcon.2009.07.001`.

[69] D. Belton, D. D. Lichti, Classification and segmentation of terrestrial laser scanner point clouds using local variance information, International Archives of Photogrammetry, Remote Sensing and Spatial Information Sciences 36 (5) (2006) 44–49.
URL `http://www.isprs.org/proceedings/xxxvi/part5/paper/BELT_619.pdf`

[70] US-DOE, EnergyPlus Home Page, 2006.
URL `http://www.eere.energy.gov/buildings/energyplus/`

[71] LBNL, Space Boundary Tool (2013).
URL `http://simulationresearch.lbl.gov/projects/space-boundary-tool`

[72] S. Lagüela, L. Díaz-Vilariño, J. Armesto, P. Arias, Non-destructive approach for the generation and thermal characterization of an as-built BIM, Construction and Building Materials 51 (2014) 55–61. `doi:10.1016/j.conbuildmat.2013.11.021`.

URL http://linkinghub.elsevier.com/retrieve/pii/S0950061813010428

[73] C. Wang, Y. K. Cho, Automated gbxml-based building model creation for thermal building simulation, in: 2014 2nd International Conference on 3D Vision, Vol. 2, 2014, pp. 111–117. doi:10.1109/3DV.2014.109.

[74] J. New, M. Adams, EnergyPlus performance improvements via JSON input refactoring, in: 2018 Building Performance Modeling Conference and SimBuild, Chicago, IL, 2018, pp. 320–324.
URL https://www.ashrae.org/File%20Library/Conferences/Specialty%20Conferences/2018%20Building%20Performance%20Analysis%20Conference%20and%20SimBuild/Papers/C044.pdf

[75] K.-H. Bae, D. D. Lichti, A method for automated registration of unorganised point clouds, ISPRS Journal of Photogrammetry and Remote Sensing 63 (1) (2008) 36 – 54, theme Issue: Terrestrial Laser Scanning. doi:https://doi.org/10.1016/j.isprsjprs.2007.05.012.
URL http://www.sciencedirect.com/science/article/pii/S0924271607000597

[76] K. Hammoudi, F. Dornaika, B. Soheilian, N. Paparoditis, Extracting outlined planar clusters of street facades from 3D point clouds, in: 2010 Canadian Conference on Computer and Robot Vision, IEEE, Ottawa, ON, Canada, 2010, pp. 122–129. doi:10.1109/CRV.2010.23.

[77] B. Okorn, X. Xiong, B. Akinci, D. Huber, Toward automated modeling of floor plans, in: Proceedings of the symposium on 3D data processing, visualization and transmission, Vol. 2, 2010.
URL https://www.ri.cmu.edu/pub_files/2010/5/2009%203DPVT%20plan%20view%20modeling%20v13%20(resubmitted).pdf

[78] E. Turner, P. Cheng, A. Zakhor, Fast, automated, scalable generation of textured 3D models of indoor environments, IEEE Journal of Selected Topics in Signal Processing 9 (3) (2015) 409–421. doi:10.1109/JSTSP.2014.2381153.